

HOSTED BY

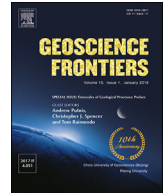


ELSEVIER

Contents lists available at ScienceDirect

China University of Geosciences (Beijing)

Geoscience Frontiers

journal homepage: [www.elsevier.com/locate/gsf](http://www.elsevier.com/locate/gsf)

Research Paper

# When will it end? Long-lived intracontinental reactivation in central Australia



Raphael Quentin de Gromard<sup>a,\*</sup>, Christopher L. Kirkland<sup>b</sup>, Heather M. Howard<sup>a</sup>,  
Michael T.D. Wingate<sup>a</sup>, Fred Jourdan<sup>b</sup>, Brent I.A. McInnes<sup>b</sup>, Martin Danišik<sup>b</sup>, Noreen J. Evans<sup>b</sup>,  
Bradley J. McDonald<sup>b</sup>, R. Hugh Smithies<sup>a</sup>

<sup>a</sup> Geological Survey of Western Australia, Department of Mines, Industry Regulation and Safety, 100 Plain Street, East Perth, WA, 6004, Australia

<sup>b</sup> School of Earth and Planetary Science/John de Laeter Centre/TIGeR, Curtin University, Perth, WA, 6845, Australia

## ARTICLE INFO

### Article history:

Received 27 April 2018

Received in revised form

20 August 2018

Accepted 18 September 2018

Available online 6 October 2018

### Keywords:

Intracontinental deformation

Thermochronology

Petermann orogen

Musgrave Province

Plate tectonics

Cratonization

## ABSTRACT

The post-Mesoproterozoic tectonometamorphic history of the Musgrave Province, central Australia, has previously been solely attributed to intracontinental compressional deformation during the 580–520 Ma Petermann Orogeny. However, our new structurally controlled multi-mineral geochronology results, from two north-trending transects, indicate protracted reactivation of the Australian continental interior over ca. 715 million years. The earliest events are identified in the hinterland of the orogen along the western transect. The first tectonothermal event, at ca. 715 Ma, is indicated by <sup>40</sup>Ar/<sup>39</sup>Ar muscovite and U–Pb titanite ages. Another previously unrecognised tectonometamorphic event is dated at ca. 630 Ma by U–Pb analyses of metamorphic zircon rims. This event was followed by continuous cooling and exhumation of the hinterland and core of the orogen along numerous faults, including the Woodroffe Thrust, from ca. 625 Ma to 565 Ma as indicated by muscovite, biotite, and hornblende <sup>40</sup>Ar/<sup>39</sup>Ar cooling ages. We therefore propose that the Petermann Orogeny commenced as early as ca. 630 Ma. Along the eastern transect, <sup>40</sup>Ar/<sup>39</sup>Ar muscovite and zircon (U–Th)/He data indicate exhumation of the foreland fold and thrust system to shallow crustal levels between ca. 550 Ma and 520 Ma, while the core of the orogen was undergoing exhumation to mid-crustal levels and cooling below 600–660 °C. Subsequent cooling to 150–220 °C of the core of the orogen occurred between ca. 480 Ma and 400 Ma (zircon [U–Th]/He data) during reactivation of the Woodroffe Thrust, coincident with the 450–300 Ma Alice Springs Orogeny. Exhumation of the footwall of the Woodroffe Thrust to shallow depths occurred at ca. 200 Ma. More recent tectonic activity is also evident as on the 21 May, 2016 (Sydney date), a magnitude 6.1 earthquake occurred, and the resolved focal mechanism indicates that compressive stress and exhumation along the Woodroffe Thrust is continuing to the present day. Overall, these results demonstrate repeated amagmatic reactivation of the continental interior of Australia for ca. 715 million years, including at least 600 million years of reactivation along the Woodroffe Thrust alone. Estimated cooling rates agree with previously reported rates and suggest slow cooling of 0.9–7.0 °C/Ma in the core of the Petermann Orogen between ca. 570 Ma and 400 Ma. The long-lived, amagmatic, intracontinental reactivation of central Australia is a remarkable example of stress transmission, strain localization and cratonization-hindering processes that highlights the complexity of Continental Tectonics with regards to the rigid-plate paradigm of Plate Tectonics.

© 2018, China University of Geosciences (Beijing) and Peking University. Production and hosting by Elsevier B.V. This is an open access article under the CC BY-NC-ND license (<http://creativecommons.org/licenses/by-nc-nd/4.0/>).

## 1. Introduction

Deformation of continental interiors, hundreds to thousands of kilometres distant from any plate margin, is a conundrum that has challenged the fundamental assumption of plate tectonics — rigid plate motion — for the last few decades (Molnar and Tappanier,

\* Corresponding author.

E-mail address: [raphael.quentindegromard@dmirs.wa.gov.au](mailto:raphael.quentindegromard@dmirs.wa.gov.au) (R. Quentin de Gromard).

Peer-review under responsibility of China University of Geosciences (Beijing).

1975; Molnar, 1988; Zoback et al., 1989; van der Pluijm et al., 1997; Marshak et al., 2000; Raimondo et al., 2014). A corollary of the rigid plate model is that deformation is localised at plate margins (McKenzie and Parker, 1967; Dewey and Bird, 1970). While this may be relatively true in oceanic settings, where indeed, plate boundaries are narrow zones with deformation almost entirely restricted to single faults or fault zones at the divergent and transform boundaries and to a relatively narrow magmatic arc at the convergent boundaries, this situation contrasts markedly with continental settings. Continental convergent plate boundaries are commonly broad orogenic zones, several hundreds of kilometres wide, within which tectonic stress is transmitted over large distances (Dewey and Bird, 1970; Molnar and Tapponnier, 1975; Tapponnier and Molnar, 1979; De Grave et al., 2007). Transmission of tectonic stress past the orogenic front is also well documented and the resulting deformation includes the formation and inversion of intracratonic sedimentary basins (van der Pluijm et al., 1997; Marshak et al., 2000; Pfiffner, 2009) and widespread intraplate seismicity (Zoback et al., 1989; Nicolas et al., 1990; Zoback, 1992). This far-field and widespread deformation is currently commonly attributed to a deformation continuum from the convergent plate margin to the continental interior, rather than the relative motion of rigid ‘platelets’ (England and McKenzie, 1982; Tapponnier et al., 1982; Molnar, 1988; van der Pluijm et al., 1997; Searle et al., 2011; Mansurov, 2017). An even more striking difference between oceanic versus continental settings in regard to the rigid plates paradigm, is the occurrence of intracontinental compressional orogens (review by Raimondo et al., 2014). These orogens occur large distances from any plate margin, and no deformation continuum exists between the plate margin and the intracontinental orogen. Such a view on intracontinental compressional orogens raises questions about the source of the stress — is it an in-plane stress generated at the plate boundary or an intraplate stress generated primarily by mantle downwelling? — and raises issues about the mechanisms of strain localization (Gorczyk et al., 2013; Raimondo et al., 2014). Raimondo et al. (2014) concluded that the stress source likely results from in-plane stress generated at the plate boundary and that the reasons for localization of intracontinental deformation reside in the mechanisms for strain localization, primarily structural heterogeneities, thermal effects, and fluid-rock interactions.

Although outnumbered by their plate margin counterparts, examples of compressional intracontinental orogens can be readily found in the literature (Raimondo et al., 2014 and references therein), and the Petermann Orogen of the Musgrave Province in central Australia provides one such example of a reactivated region that has an important tectonic history long after collision and suturing (Hand and Sandiford, 1999; Camacho and McDougall, 2000; Aitken et al., 2009a, b; Raimondo et al., 2010; Raimondo et al., 2014; Glorie et al., 2017). The initial collision in the Musgrave Province is interpreted to have occurred during the 1310–1293 Ma Mount West Orogeny that marks the final docking of the North, West, and South Australian Cratons (NAC, WAC, SAC, respectively) (Howard et al., 2015; Kirkland et al., 2015). Since final amalgamation of the NAC, WAC, and SAC, several magmatic and amagmatic tectonic events have reworked their common suture. In the Musgrave Province, intracontinental tectonomagmatic events include the 1220–1150 Ma Musgrave Orogeny and the 1085–1030 Ma Giles Event (Kirkland et al., 2013; Howard et al., 2015; Smithies et al., 2015a, b). The most pronounced and widely recognised post-magmatic intracontinental event is the 580–520 Ma Petermann Orogeny, which exhumed the Musgrave Province and produced an 800 km long and 300 km wide, east-trending, positive gravity anomaly in central Australia (Lambeck and Burgess, 1992; Camacho and McDougall, 2000; Aitken et al., 2009a).

Nevertheless, the post-Mesoproterozoic exhumation history of the Musgrave Province remains poorly understood. In the absence of extensive magmatism, constraining the evolution of an orogen is challenging, but can be addressed through multi-isotope thermochronology, where different minerals and isotopic systems have different susceptibilities to overprinting or cooling through different time-temperature points. Such post peak temperature data are rare in the Musgrave Province and mostly from the central and eastern parts (Tingate, 1990; Camacho and Fanning, 1995; Camacho, 1997; Scrimgeour et al., 1999; Gregory et al., 2009; Walsh et al., 2013; Glorie et al., 2017). In the west Musgrave Province, the only thermochronology data available is from the Bates region, core of the Petermann Orogen (Raimondo et al., 2009, 2010). A multi-isotope study across the west Musgrave Province is therefore needed in order to elucidate the post-Mesoproterozoic, post-magmatic, reworking events and, more broadly, to better understand the processes of evolution of intracontinental deformation. In the current contribution, we present U–Pb zircon and titanite data, combined with  $^{40}\text{Ar}/^{39}\text{Ar}$  hornblende, muscovite, and biotite data, and zircon (U–Th)/He data, collected along two approximately north-trending transects in the west Musgrave Province, from rocks affected by the latest phases of deformation in order to constrain the post-magmatic tectonic evolution of this region. We combine this extensive thermochronology with the results of recent regional mapping in the west Musgrave Province.

## 2. Geology of the west Musgrave Province

The Musgrave Province is an east-trending Mesoproterozoic orogen exposed at the junction between the NAC, SAC, and WAC and bounded by the younger Amadeus and Officer Basins to the north and south, respectively (Figs. 1 and 2). The province forms a gravity and magnetic anomaly about 550 km long and 250 km wide along the South Australia and Northern Territory border and extends westward in Western Australia for another 300 km, where it is named the west Musgrave Province.

The oldest known rocks in the Musgrave Province are 1600–1500 Ma felsic volcanic, sedimentary, and intrusive rocks

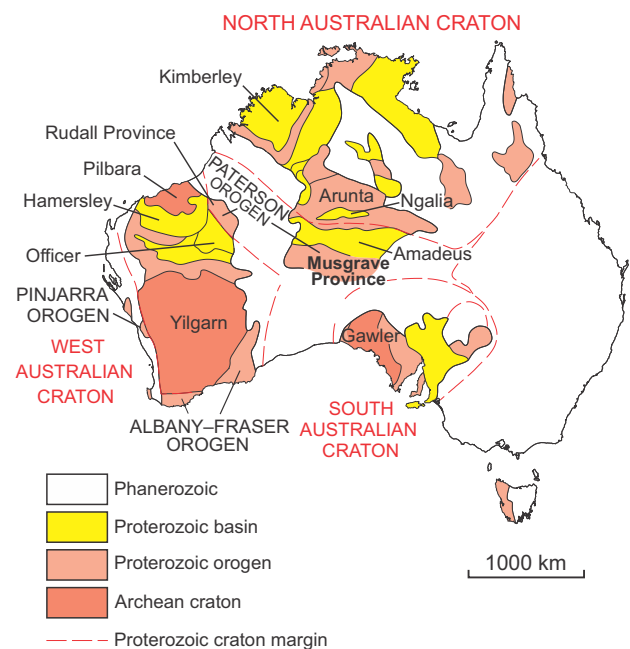


**Figure 1.** Tectonic map of Australia showing the location of the Proterozoic Musgrave Province at the junction between the North, West and South Australian Cratons.



**Table 1**  
Summary of thermochronology data for the western Musgrave Province. Easting and Northing for sample locations are given using Map Grid of Australia (MGA) coordinates, Zone 52. The column 'Temperature' is that used for the Y-axis of Fig. 8b. The temperatures for the interpreted cooling ages are the closure temperatures of the method for the mineral considered; those for the interpreted metamorphic ages are from published Zr-in-titanite and Ti-in-zircon thermometry data where available. References: 1 (this study); 2 (Tingate, 1990); 3 (Walsh et al., 2013); 4 (Scrimgeour et al., 1999); 5 (Raimondo et al., 2009); 6 (Close et al., 2003); 7 (Gregory et al., 2009); 8 (Raimondo et al., 2010).

Sample No.	Location, lithology	Easting	Northing	Mineral	Interpretation	Age (Ma)	Uncertainty (Ma)	Temperature (°C)	Reference
<b>Fission track</b>									
8551-37	Pottoyu Suite granite	565,300	7,227,900	apatite	cooling	271	15	95 ± 15	2
8551-35	Pottoyu Suite granite	607,700	7,226,000	apatite	cooling	327	28	95 ± 15	2
8551-38	Larapinta Group	607,600	7,225,900	apatite	cooling	341	58	95 ± 15	2
<b>(U–Th)/He</b>									
208486	South Wankari Detachment, migmatitic granite	498,403	7,205,741	zircon	cooling	197	37	185 ± 35	1
180299	Bates region, metagranite	499,043	7,138,416	zircon	cooling	397	22	185 ± 35	1
174737	Bates region, metagranite	460,511	7,147,960	zircon	cooling	480	48	185 ± 35	1
208529	Nyingana Range, Dean Quartzite	453,297	7,271,388	zircon	cooling	531	72	185 ± 35	1
208530	Bloods Range, Dean Quartzite	477,485	7,260,757	zircon	cooling	546	52	185 ± 35	1
<b><sup>40</sup>Ar/<sup>39</sup>Ar</b>									
208501	Wanarn area, paragneiss	347,878	7,200,267	biotite	cooling	584	3	365 ± 35	1
208488	Dog Leg Anticline, Qz-Ms schist	493,139	7,221,001	muscovite	cooling	552	3	425 ± 70	1
208421	Bedford Range, Ms-Bt schist	320,617	7,217,390	muscovite	cooling	566	3	425 ± 70	1
208403	Mitika area, Ms-Gt Schist	314,196	7,174,200	muscovite	cooling	587	3	425 ± 70	1
208407	Mitika area, Ms-Gt Schist	315,523	7,170,290	muscovite	cooling	593	3	425 ± 70	1
208418	North Mitika area, Ms-Gt Schist	332,861	7,180,508	muscovite	cooling	613	2	425 ± 70	1
185414	South Mitika area, Quartzite	315,618	7,151,266	muscovite	cooling	623	5	425 ± 70	1
194794	Talbot Sub-basin, mylonitic schist	309,164	7,109,161	muscovite	crystallization	712	10	-	1
194796	Talbot Sub-basin, mylonitic schist	307,040	7,108,063	muscovite	crystallization	713	8	-	1
194795	Talbot Sub-basin, mylonitic schist	309,146	7,109,162	muscovite	crystallization	718	6	-	1
208420	Bedford Range, amphibolite	321,972	7,220,235	hornblende	cooling	589	4	585 ± 50	1
<b>K–Ar</b>									
P90/477	Piltardi Detachment Zone, Dean Quartzite	565,200	7,232,100	muscovite	cooling	568	5	425 ± 70	4
P89/1310	Piltardi Detachment Zone, Dean Quartzite	596,300	7,208,600	muscovite	cooling	586	5	425 ± 70	4
PR96IRS563	Mantapayika Granite, migmatitic gneiss	520,300	7,165,500	hornblende	metamorphism/cooling	565	9	-	4
<b>Rb–Sr</b>									
PRG1	Pottoyu Suite granite	591,000	7,196,300	biotite	cooling	570	50	350 ± 50	4
PRG3	Pottoyu Suite granite	607,000	7,190,200	biotite	cooling	600	50	350 ± 50	4
<b>Sm–Nd</b>									
PR96IRS532A	Mann Ranges, recrystallised dolerite	590,900	7,147,700		cooling	494	59	600 ± 50	4
PR95IRS188	Olia Chain region, recrystallised dolerite	622,150	7,168,068		metamorphism	550	11	-	6
<b>U–Pb</b>									
441	Western Mann Ranges, mylonitic mafic dyke	546,600	7,124,275	rutile	cooling	472	20	555 ± 5	3
Pe9	Cockburn Shear Zone, metagranite	543,128	7,127,326	rutile	cooling	498	18	555 ± 5	3
DFC387	Western Mann Ranges, mylonitic mafic dyke	550,625	7,125,847	rutile	cooling	519	15	555 ± 5	3
195231	Talbot Sub-basin, metagranite	315,907	7,118,628	titanite	metamorphism	715	7	-	1
187323	Bates region, mylonite	480,390	7,157,417	titanite (large grains)	metamorphism	572	7	734 ± 20	5, 8
187337	Bates region, mylonite	486,861	7,149,675	titanite (large grains)	metamorphism	573	14	748 ± 20	5, 8
184495	Bates region, mylonite	491,863	7,140,895	titanite (small grains)	cooling	539	4	630 ± 30	5
155731	Bates region, mylonite	486,733	7,146,105	titanite (small grains)	cooling	552	12	630 ± 30	5
Pe24	Cockburn Shear Zone area, metagranite	543,137	7,127,755	titanite	cooling	521	8	630 ± 30	3

**Table 1** (continued)

Sample No.	Location, lithology	Easting	Northing	Mineral	Interpretation	Age (Ma)	Uncertainty (Ma)	Temperature (°C)	Reference
Pe9	Cockburn Shear Zone, metagranite	543,128	7,127,326	titanite	cooling	551	21	630 ± 30	3
460a	Western Mann Ranges, mylonitic mafic dyke	530,550	7,134,650	titanite	cooling	564	22	630 ± 30	3
DFC507	40 km north of Mann Ranges, metagranite	524,127	7,165,281	titanite	cooling	567	18	630 ± 30	3
Pe13	Cockburn Shear Zone, leucosome	543,279	7,127,973	allanite (cores)	metamorphism	559	6	735 ± 15	7
Pe13	Cockburn Shear Zone, leucosome	543,279	7,127,973	allanite (rims)	cooling	551	6	650 ± 50	7
187323	Bates region, mylonite	480,390	7,157,417	zircon (rim) (LA-ICPMS)	metamorphism	574	5	719 ± 8	8
205194	Mitika Area, paragneiss	315,092	7,169,701	zircon (rim)	metamorphism	628	4	-	1
208414	Mitika area, quartzite	313,654	7,172,427	zircon (rim)	metamorphism	631	12	-	1
PR96IRS549	Umutju region, migmatite	533,390	7,165,850	zircon (rim)	metamorphism	561	11	700 ± 50	4
Pe13	Cockburn Shear Zone, leucosome	543,279	7,127,973	zircon (rim)	metamorphism	555	7	735 ± 15	7
Pe24	Cockburn Shear Zone area, metagranite	543,137	7,127,755	zircon (rim)	metamorphism	544	7	740 ± 20	3
155735	Bates region, mylonite	486,644	7,146,037	zircon (rim)	metamorphism	568	12	794 ± 12	8
208482	South Wankari Detachment, pegmatite	493,974	7,205,619	zircon	crystallization	573	8	-	1
208505	Wanarn area, pegmatite	332,532	7,205,154	zircon	crystallization	592	6	-	1

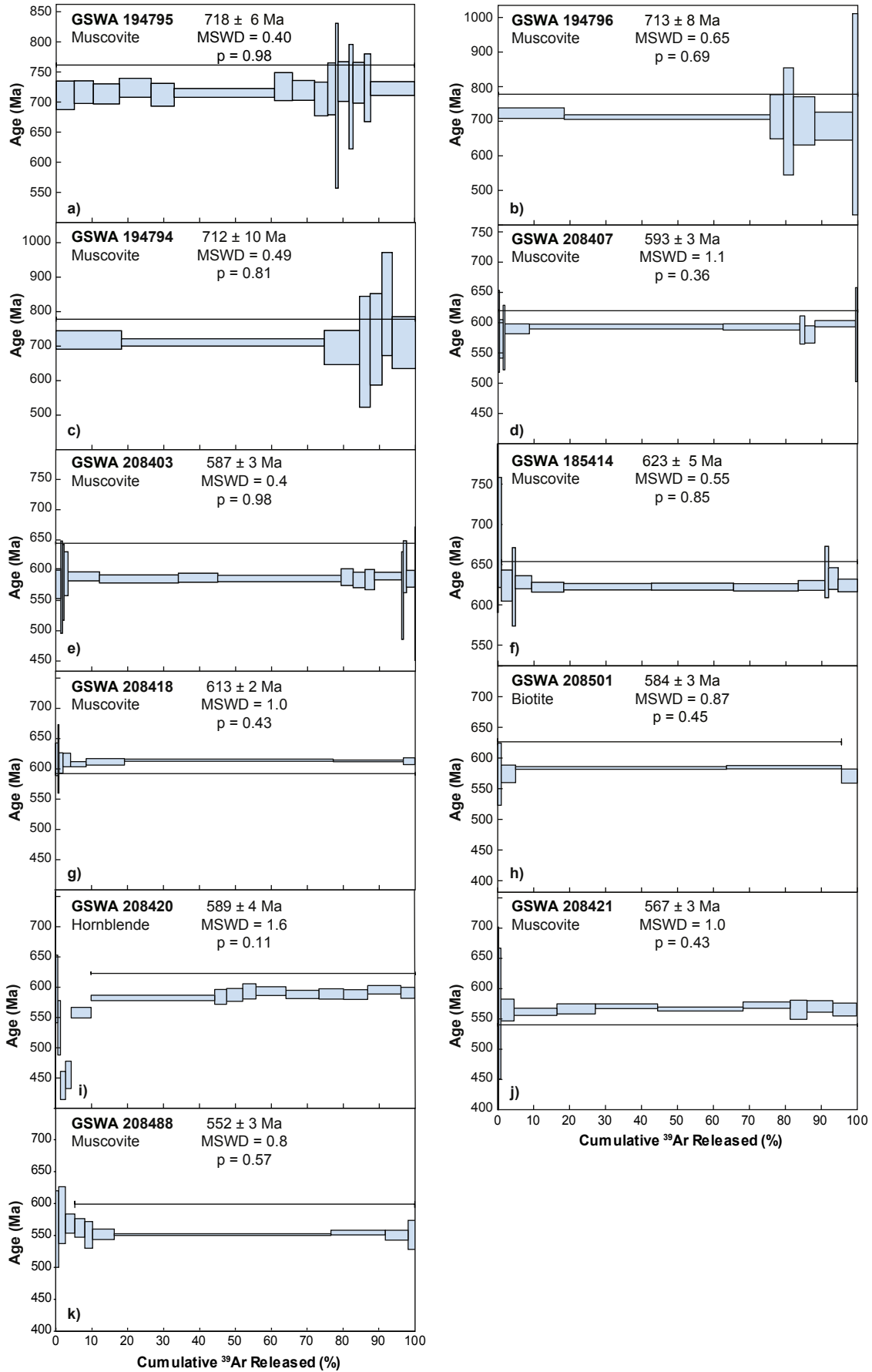
Notes: 1. All uncertainties are given at 95% confidence.

(Gray, 1978; Major and Conor, 1993; Camacho and Fanning, 1995; Edgoose et al., 2004; Howard et al., 2015), including the poorly exposed ca. 1600 Ma Warlawurru Supersuite of the west Musgrave Province (Fig. 2; Quentin de Gromard et al., 2016b). Although, an older crustal component generated at ca. 1900 Ma has been inferred for the region based on Nd and Hf isotopic studies (Kirkland et al., 2017). The Mount West Orogeny is the oldest major tectono-magmatic event identified in the west Musgrave Province, and is characterised by emplacement of subduction-derived magmatic rocks of the 1345–1293 Ma Wankanki Supersuite and deposition of volcano-sedimentary rocks of the 1340–1270 Ma Wirku Metamorphics (Fig. 2) in a continental arc setting (Smithies et al., 2010; Evins et al., 2012; Howard et al., 2015). The subsequent Musgrave Orogeny included emplacement of voluminous mantle-derived granitic magmas of the 1220–1150 Ma Pitjantjatjara Supersuite (Fig. 2) accompanied by prolonged ultra-high temperature (UHT) crustal conditions (Edgoose et al., 2004; Smithies et al., 2011, 2015b). A post-subduction mantle lithosphere delamination process following the Mount West Orogeny may explain the unusually elevated and prolonged heat flow of the Musgrave Orogeny (Gorczyk et al., 2015).

The youngest major magmatic event recorded in the Musgrave region is the 1085–1030 Ma Giles Event (Smithies et al., 2009). The Giles Event initiated with deposition of siliciclastic sediments of the MacDougall Formation and widespread eruption of the intracontinental rift-related Mummawarrawarra Basalt (together forming the Kunmarnara Group; Fig. 2) into the failed Nganyatjarra Rift (Evins et al., 2010). Igneous rocks formed during the Giles Event belong to the Warakurna Supersuite and include the giant layered mafic-ultramafic Giles intrusions, mixed and mingled gabbros and leucogranites, Alcurra Dolerite intrusions, and bimodal volcanic rocks of the Talbot Supervolcano (Fig. 2) (Howard et al., 2009; Evins et al., 2010; Smithies et al., 2015a). The Giles Event encompasses the more extensive and short-lived Warakurna Large Igneous Province (Wingate et al., 2004) and is likely the result of tectonic processes including the thermal heritage of the Musgrave Orogeny together with sinistral strike-slip movement along the continent-scale Mundrabilla Shear Zone (Smithies et al., 2015b).

Apart from minor mafic dyke intrusion at ca. 1000 Ma, 825 Ma and 750 Ma (Glikson et al., 1996; Wingate et al., 1998; Howard et al., 2007), the Musgrave Province is commonly regarded as tectonically quiescent until intracontinental reactivation during the 580–520 Ma Petermann Orogeny. Deformation during the Petermann Orogeny produced east-trending crustal-scale faults and shear zones that dissect the entire Musgrave Province, the most prominent of which include the Mann Fault and the Woodroffe Thrust (inset of Fig. 2; Bell, 1978; Lambeck and Burgess, 1992; Camacho and McDougall, 2000; Aitken et al., 2009a; Wex et al., 2017). Tectonic transport during the Petermann Orogeny is largely towards the north, which interleaved rocks of the Musgrave Region with the basal sedimentary sequence of the Amadeus Basin, notably within the Petermann Nappe Complex (Fig. 2; Scrimgeour et al., 1999; Edgoose et al., 2004; Flöttmann et al., 2004).

Peak metamorphic conditions during the Petermann Orogeny were attained in the hanging wall of the Woodroffe Thrust and approached eclogite facies ( $P = 10\text{--}14$  kbar and  $T = 700\text{--}800$  °C) at ca. 570 Ma (Scrimgeour and Close, 1999; Edgoose et al., 2004; Raimondo et al., 2010). The existence of regional-scale, flat-lying mylonitic fabrics with opposing sense of shear, which developed over a prolonged deformation history and at slow cooling rates, is consistent with a crustal channel flow model for the exhumation of the orogenic core, similar to that proposed for the Himalayan–Tibetan system (Raimondo et al., 2009, 2010; Walsh et al., 2013). Metamorphic conditions attributed to the Petermann Orogeny decrease from amphibolite facies in the footwall of the Woodroffe Thrust in the south to lower greenschist facies in the northern Petermann Nappe Complex (Fig. 2; Scrimgeour et al., 1999).  $P\text{--}T$  estimates immediately north of the Woodroffe Thrust are ca. 6–7 kbar and ca. 650 °C at ca. 550 Ma (Scrimgeour and Close, 1999; Edgoose et al., 2004). Evidence for deformation related to the 450–300 Ma Alice Springs Orogeny is rare; however, apatite fission track ages of 388–271 Ma from the Petermann Nappe Complex in the central Musgrave Province indicate cooling that correlate with the timing of the latest stage of the Alice Springs Orogeny (Tingate, 1990; Edgoose et al., 2004). In the eastern Musgrave Province, apatite fission track and (U–Th)/He apatite and zircon dates of ca. 450–400 Ma and ca. 310–290 Ma



are interpreted to represent exhumation related to the Alice Springs Orogeny (Glorie et al., 2017).

### 3. Structure of the west Musgrave Province and new thermochronology results

Samples were collected along two approximately north-trending transects across the main structures that define the hinterland, core, and foreland of the Petermann Orogen in the west Musgrave Province (Fig. 2). The western transect extends from the hinterland (south of the Mitika Fault), to the core of the orogen (region between the Mitika Fault and the Woodroffe Thrust); the eastern transect extends from the core of the orogen (region between the Mann Fault and the Woodroffe Thrust) to the foreland fold and thrust belt in the Petermann Ranges (Fig. 2). All age uncertainties cited in this paper are reported at the 95% confidence level, unless otherwise indicated. The analytical procedures, sample descriptions and geochronology results, as well as the data tables for  $^{39}\text{Ar}/^{40}\text{Ar}$ , U–Pb zircon and titanite and (U–Th)/He zircon analyses are provided in appendices (Appendix A,B; Tables A1–A4, respectively). A summary table including new and previously published geochronology data is presented in Table 1.

#### 3.1. Western transect

Thermochronology results along the western transect include U–Pb zircon and titanite data and  $^{40}\text{Ar}/^{39}\text{Ar}$  hornblende, muscovite, and biotite data. We observe an overall younging of ages from south to north (Fig. 2). The structure of the southernmost hinterland — the Talbot Sub-basin — is characterized by a regional, west- to northwest-trending, open anticline with south-directed reverse faults disrupting its northern limb (Fig. 2; Howard et al., 2014; Quentin de Gromard et al., 2015). Muscovite  $^{40}\text{Ar}/^{39}\text{Ar}$  analyses of three muscovite–(kyanite)–(andalusite) schists, collected along strike of the Talbot Sub-basin anticline, yield dates of  $718 \pm 6$  Ma,  $713 \pm 8$  Ma, and  $712 \pm 10$  Ma (GSWA 194794,5,6; Figs. 2 and 3a–c; Table 1). The primary crystallization temperature of muscovite in these samples is difficult to estimate and is likely close to the closure temperature of the argon isotopic system in muscovite. Muscovite grains from these samples are either associated with andalusite or kyanite, suggesting that muscovite growth did not exceed ca.  $500^\circ\text{C}$  (temperature of the alumino-silicate triple point) as indicated by the lack of sillimanite. Igneous zircon crystals from a nearby metagranitic rock yield a U–Pb date of  $1079 \pm 8$  Ma, interpreted as the time of crystallization of the granite protolith (GSWA 195231; Figs. 2 and 4a; Table 1). Laser-ablation ICPMS U–Pb titanite dates from the same metagranite sample are bimodal (Fig. 5). One group indicates dates of ca. 1100 Ma to 942 Ma, interpreted as the time the granite cooled below ca.  $600^\circ\text{C}$  (the Pb retention temperature in titanite; Frost et al., 2001). The second group of titanite analyses yields an age peak at  $715 \pm 7$  Ma, interpreted as the age of metamorphic growth of titanite. Because of the similarity between the U–Pb titanite and  $^{40}\text{Ar}/^{39}\text{Ar}$  muscovite dates, we favour the interpretation of the ca. 715 Ma  $^{40}\text{Ar}/^{39}\text{Ar}$  muscovite dates as representing the age of muscovite crystallization.

The northern hinterland area around Mitika records development of a west- to northwest-verging fold and thrust system (Fig. 2; Howard et al., 2013). The age of peak metamorphism is indicated by U–Pb dates of  $631 \pm 12$  Ma and  $628 \pm 4$  Ma for metamorphic rims around detrital zircons from two garnet-kyanite metasedimentary samples (GSWA 208414, 205194) of the Kunmarnara Group

collected from the core of the fold and thrust system (Figs. 2 and 4b,c; Table 1). Muscovite bearing samples, collected from the same area, yielded  $^{40}\text{Ar}/^{39}\text{Ar}$  plateau ages of  $593 \pm 3$  Ma and  $587 \pm 3$  Ma (GSWA 208403, 208407; Figs. 2 and 3d,e; Table 1). Based on the muscovite-garnet-kyanite amphibolite facies metamorphic assemblage, the high-temperature quartz deformation and recovery temperature estimates (e.g. chessboard patterns  $>600^\circ\text{C}$ ; Kruhl, 1996) and the high-temperature grain boundary migration recrystallization in quartz ( $>530^\circ\text{C}$ ; Stipp et al., 2002) post-dating muscovite growth, we interpret the  $^{40}\text{Ar}/^{39}\text{Ar}$  muscovite dates from the core of the fold and thrust system to reflect cooling ages. Hence, that core of the fold and thrust system cooled below ca.  $425^\circ\text{C}$  (the retention temperature of argon in muscovite; Scibiorski et al., 2015) at ca. 590 Ma. Two samples collected from the southern and northern periphery of the fold and thrust system yielded  $^{40}\text{Ar}/^{39}\text{Ar}$  muscovite dates of  $623 \pm 5$  Ma and  $613 \pm 2$  Ma, respectively (GSWA 185414, 208418; Figs. 2 and 3f,g; Table 1). Both samples contain quartz displaying textural evidence of a high-temperature deformation and recovery process (e.g. chessboard patterns  $>600^\circ\text{C}$ ; Kruhl, 1996). Quartz recrystallization post-dating muscovite growth is dominated by subgrain rotation recrystallization, but grain boundary migration recrystallization is also commonly present, suggesting that quartz recrystallization occurred within the  $480^\circ\text{C}$  to  $530^\circ\text{C}$  range, using the recrystallization thermometer of Stipp et al. (2002). All of the above observations suggests that the temperature during peak metamorphism exceeded the argon retention temperature in muscovite of ca.  $425^\circ\text{C}$ . There is no evidence of muscovite growth postdating peak metamorphic conditions, thus, the  $^{40}\text{Ar}/^{39}\text{Ar}$  plateau ages of  $623 \pm 5$  Ma and  $613 \pm 2$  Ma are interpreted as the age of cooling of the samples below ca.  $425^\circ\text{C}$ . This indicates that the lower-grade periphery of the Mitika area cooled below ca.  $425^\circ\text{C}$  between  $623 \pm 5$  Ma and  $613 \pm 2$  Ma.

The gneissic core of the orogen, in the area around Wanarn, is a zone of complex ductile deformation where basement rocks of the Musgrave Province are tectonically interleaved with rocks of the Kunmarnara Group (Quentin de Gromard et al., 2016a). The resulting geometry is a regional-scale antiformal stack bounded to the south by the Mitika Fault and to the north by the Woodroffe Thrust (Quentin de Gromard et al., 2017a, b). Pegmatite veins intruding the Kunmarnara Group yield U–Pb zircon crystallization ages of  $592 \pm 6$  Ma (GSWA 208505; Figs. 2 and 4d; Table 1). A biotite-bearing quartzofeldspathic paragneiss collected from the central Wanarn area yielded a  $^{40}\text{Ar}/^{39}\text{Ar}$  biotite date of  $584 \pm 3$  Ma (GSWA 208501; Figs. 2 and 3h; Table 1). Feldspar grains from this sample show crystal plastic intracrystalline deformation in the form of undulose extinction and deformation twinning. Recrystallization occurred during both bulging and subgrain rotation recrystallization processes. This indicates deformation and recrystallization temperatures above  $600^\circ\text{C}$  (Passchier and Trouw, 1996, and references therein). Quartz microstructures display ubiquitous chessboard pattern subgrain boundaries ( $T > 600^\circ\text{C}$ ; Kruhl, 1996) and recrystallization was largely dominated by high-temperature grain boundary migration recrystallization. Only one generation of biotite could be identified by optical microscopy. Biotite is deformed and there is no evidence for biotite grains post-dating deformation and recrystallization of the surrounding quartz-feldspar matrix. We interpret these textural relationships to indicate that temperatures were well above the closure temperature of argon in biotite (ca.  $365^\circ\text{C}$ ; Scibiorski et al., 2015) after biotite growth, which implies that the biotite  $^{40}\text{Ar}/^{39}\text{Ar}$  plateau age of

**Figure 3.**  $^{40}\text{Ar}/^{39}\text{Ar}$  step-heating spectra for samples employed in this study. Individual steps are graphed against cumulative percentage of  $^{39}\text{Ar}$  released. Uncertainties are given at  $2\sigma$  for plateau ( $>70\%$  of  $^{39}\text{Ar}$  released) ages. The MSWD and probability (p) are given for plateau ages. All samples yielded statistically robust age plateaus ( $>90\%$  of  $^{39}\text{Ar}$  released). Analytical procedures and summary of  $^{40}\text{Ar}/^{39}\text{Ar}$  thermochronology results are given in Appendix A and Table A1 respectively.

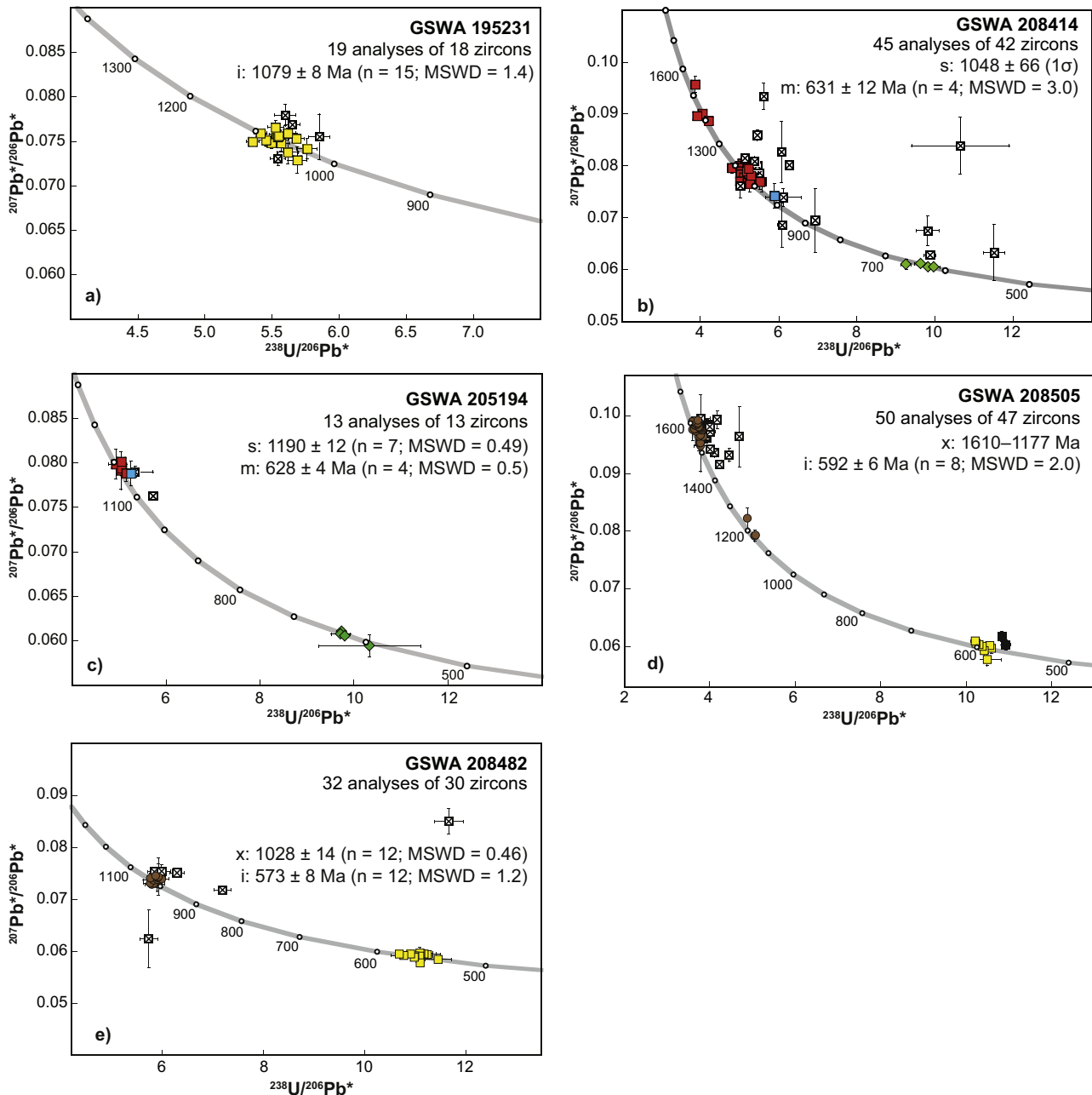


**Figure 4.** U–Pb analytical data for zircons from samples employed in this study. Yellow squares indicate analyses of igneous zircons; blue squares indicate the youngest detrital zircon; red squares indicate older detrital zircons; green diamonds indicate metamorphic zircons; brown circles indicate xenocrystic zircons; black squares indicate radiogenic-Pb loss; crossed squares indicate data excluded because of discordance >5% or high common Pb. i: igneous crystallization age; s: maximum depositional age; m: metamorphic age; x: ages of xenocrystic components.

584 ± 3 Ma dates the time of cooling of this sample below its retention temperature of ca. 365 °C. An amphibolite sample from the northwestern end of the Wanarn area yielded an amphibole  $^{40}\text{Ar}/^{39}\text{Ar}$  plateau age of 589 ± 4 Ma (GSWA 208420; Figs. 2 and 3i; Table 1). The mineral phases in equilibrium during peak metamorphism consist of the assemblage hornblende–sillimanite–rutile suggesting upper amphibolite facies conditions. Plagioclase was recrystallised by subgrain rotation processes suggesting recrystallization temperatures of temperature above 600 °C (Passchier and Trouw, 1996, and references therein). There is no evidence for hornblende recrystallization or neocrystallization following peak metamorphic conditions, thus the plateau age of 589 ± 4 Ma is interpreted as the age of cooling

below the retention temperature of argon in hornblende (ca. 585 °C; Scibiorski et al., 2015). A muscovite–biotite sample collected from the same area in the northwestern end of the Wanarn area yielded a  $^{40}\text{Ar}/^{39}\text{Ar}$  plateau age of 567 ± 3 Ma (GSWA 208421; Figs. 2 and 3j; Table 1). Multiple generations of muscovite might be present as several orientations can be defined, but none appear to post-date the deformation and recrystallization that affected quartz and K-feldspar grains in the surrounding matrix. K-feldspar grains are internally deformed and show evidence of crystal plastic deformation. Quartz grains display ubiquitous chessboard subgrain boundaries and their recrystallization is largely dominated by the high-temperature grain boundary migration process. Pinning structures of quartz grains around

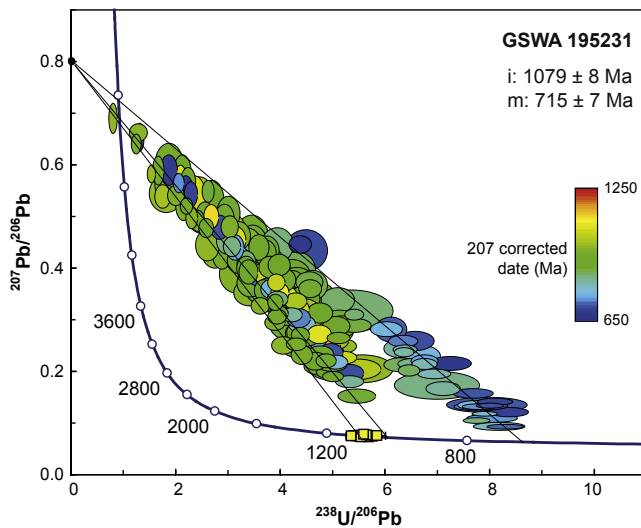


**Figure 5.** Laser-ablation ICPMS U–Pb titanite and SHRIMP U–Pb data for sample GSWA 195231; ellipses ( $2\sigma$ ) indicate titanite data; yellow squares represent SHRIMP analyses of igneous zircons (Fig. 4a). Lines represent approximate mixing lines between common and radiogenic Pb components.

muscovite indicate that deformation and recrystallization temperatures of over 600 °C postdate muscovite growth (Jessell, 1987). Therefore, the plateau age of  $567 \pm 3$  Ma is interpreted as the age of cooling below the retention temperature of argon in muscovite (ca. 425 °C; Scibiorski et al., 2015). From all of the above, we can conclude that the central part of the Wanarn area cooled below ca. 365 °C at  $584 \pm 3$  Ma, whereas the northwestern part of the Wanarn area cooled below ca. 585 °C at  $589 \pm 4$  Ma and then below ca. 425 °C at  $567 \pm 3$  Ma.

### 3.2. Eastern transect

New thermochronology along this transect includes U–Pb zircon,  $^{40}\text{Ar}/^{39}\text{Ar}$  muscovite and (U–Th)/He zircon data (Fig. 2). The area towards the foreland — commonly referred to as the Petermann Nappe Complex — is a zone characterised by folding, basal decollement, fault imbrication and duplexing, and a backthrust zone, all classic features of a foreland fold and thrust belt (Scrimgeour et al., 1999; Edgoose et al., 2004; Flöttmann et al., 2004; Quentin de Gromard et al., 2017b). In this area, basement rocks of the Musgrave region are tectonically interleaved with the basal sedimentary sequence of the Amadeus Basin, with metamorphic grade decreasing from south to north from amphibolite to sub-greenschist facies (Scrimgeour et al., 1999; Scrimgeour and Close, 1999; Edgoose et al., 2004; Quentin de Gromard et al., 2017b).

A pegmatite sample collected approximately 15 km south of the Wankari Detachment — regarded as the southern end of the Petermann Nappe Complex (Edgoose et al., 2004) — yields a U–Pb zircon crystallization age of  $573 \pm 8$  Ma (GSWA 208482; Figs. 2 and 4e; Table 1). One kilometre north of the Wankari Detachment, within the Dog Leg Anticline, a quartz–muscovite schist yields an  $^{40}\text{Ar}/^{39}\text{Ar}$  muscovite date of  $552 \pm 3$  Ma (GSWA 208488; Figs. 2 and 3k; Table 1). Near the sample site, minor pelitic horizons exist within the succession and contain kyanite–muscovite–biotite assemblages (also described in Scrimgeour et al., 1999). Interlayered mafic volcanic rocks now consist of mafic amphibolites, with amphibole needles up to one centimetre long. No PT estimates were obtained directly from the Dog Leg Anticline, but rocks on the southern and northern side of the Wankari Detachment,

approximately 60–100 km to the east, yielded PT estimates of 6.5 kbar and 640 °C and 6.3 kbar and 610 °C, respectively (Scrimgeour and Close, 1999). This strongly suggests that the  $552 \pm 3$  Ma  $^{40}\text{Ar}/^{39}\text{Ar}$  muscovite date from the Dog Leg Anticline reflects the time of cooling below ca. 425 °C. Two sandstone samples collected in the backthrust zone at the northern end of the Petermann Nappe Complex, yield (U–Th)/He zircon dates between 618–513 Ma ( $n = 5$ ; mean date of  $546 \pm 52$  Ma, MSWD = 2.0) and 641–483 Ma ( $n = 5$ ; mean date of  $531 \pm 72$  Ma, MSWD = 2.1), respectively (GSWA 208529, 208530; Figs. 2 and 6; Table 1), taken as time of cooling through the 150–220 °C He retention temperature in zircon (Reiners et al., 2002, 2004).

Two samples collected in the core of the orogen yield (U–Th)/He zircon dates younger than the 580–530 Ma Petermann Orogeny (Fig. 2). On the western side of the Mount Fanny Fault, a metazonogranite sample (GSWA 174737) yielded dates of 541–438 Ma ( $n = 5$ ; mean date of  $480 \pm 48$  Ma, MSWD = 1.4) and on the eastern side of the Mount Fanny Fault, a metagranite sample (GSWA 180299) yields dates of 421–370 Ma ( $n = 5$ ; mean date of  $397 \pm 22$  Ma, MSWD = 0.47) (Figs. 2 and 6; Table 1). A metasyenogranite sample (GSWA 208486), collected 15 km south of the Wankari Detachment and along strike from pegmatite sample GSWA 208482 yields (U–Th)/He zircon dates of 248–154 Ma with a mean date of  $197 \pm 37$  Ma ( $n = 6$ ; MSWD = 2.1) (Figs. 2 and 6; Table 1). As in the case of the samples from the northern end of the Petermann Nappe Complex, these results are considered to indicate the time of cooling through 150–220 °C, which is our preferred

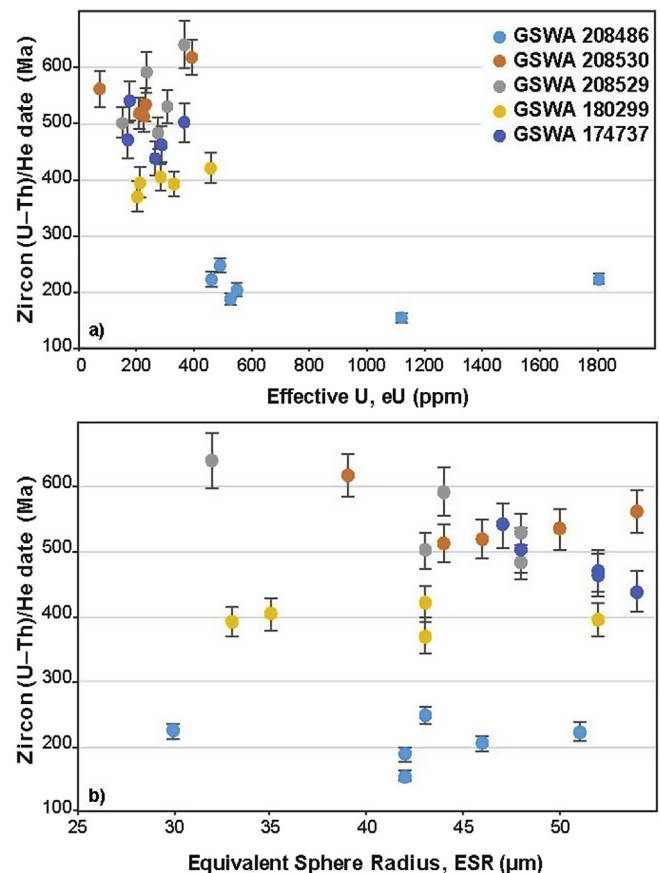


**Figure 6.** (a) Zircon (U–Th)/He date vs. effective uranium content where  $eU$  (ppm) = U concentration +  $0.235 \times$  Th concentration; this parameter is commonly used in thermochronology as a proxy for radiation damage. Error bars are  $1\sigma$ . (b) Zircon (U–Th)/He date vs. Equivalent Sphere Radius (ESR).

interpretation given the lack of geological constraints and is the most conservative interpretation. We do, however, acknowledge that ZHe dates may reflect apparent ages resulting from a partial rejuvenation of the (U–Th)/He system by later thermal event(s) (e.g. Danišik et al., 2015).

## 4. Discussion

### 4.1. 500 Ma of amagmatic intracontinental reactivation

Thermochronology data from the western transect indicate about 150 million years of pre- to syn-Petermann Orogeny tectonometamorphic history (Figs. 7 and 8a). Two previously inferred deformation and metamorphic events are here dated at ca. 715 Ma and 630 Ma and indicate that the post-Mesoproterozoic amagmatic intracontinental reactivation of the Musgrave Province started during the Cryogenian. The ca. 715 Ma metamorphic event is interpreted to result from thickening of the Talbot Sub-basin during N–S compression (Fig. 2; Howard et al., 2014; Quentin de Gromard et al., 2015), while the ca. 630 Ma event results from the development of the north-trending fold and thrust system during E–W compression (Howard et al., 2013). The different compression direction and the 85 million year time gap between these two events are inconsistent with a single continuous event (Fig. 8a). On the other hand, high-temperature conditions, indicated by metamorphic zircon growth at ca. 630 Ma, were followed closely by cooling during uplift of the lower-grade periphery of the Mitika area at ca. 623 Ma and 613 Ma (Figs. 7 and 8a). The higher-grade core of the fold and thrust system of the Mitika area (Fig. 2) in

turn cooled below ca. 425 °C at ca. 590 Ma. This is broadly contemporaneous with cooling of the Wanarn area, which was exhumed along the Woodroffe Thrust (e.g. CDE cross section of DIORITE, Quentin de Gromard et al., 2016a). The Wanarn area is traversed by major thrusts that display differential cooling across them. The central part of the orogenic core, near Wanarn (Fig. 2), cooled below ca. 365 °C at ca. 584 Ma ( $^{40}\text{Ar}/^{39}\text{Ar}$  biotite cooling age), while the northwest corner was still at ca. 585 °C and further cooled to ca. 425 °C at 565 Ma ( $^{40}\text{Ar}/^{39}\text{Ar}$  hornblende and muscovite ages, respectively; Figs. 7 and 8a). This suggests differential cooling of the Wanarn area during development of the regional antiformal stack and generation of minor granitic melt as indicated by the age of pegmatite intrusion at  $592 \pm 6$  Ma during exhumation. Several closely spaced cooling ages between ca. 630 Ma and 565 Ma clearly show a continuous exhumation of the western transect area resulting from the orogenic process. We therefore propose that the Petermann Orogeny started as early as 630 Ma. In this case, much of the existing thermochronology data for the Musgrave Province can be linked to thermal events related to a redefined 630–520 Ma Petermann Orogeny (Fig. 8a).

Along the eastern transect, thermochronology data across the orogenic core into the foreland fold and thrust belt indicate a younger tectonometamorphic history (Figs. 7 and 8a). Peak metamorphic conditions (10–14 kbar, 700–800 °C) in the core of the orogen were attained at ca. 570 Ma as indicated by U–Pb dates from cores of large titanite grains and from zircon rims (Raimondo et al., 2009, 2010). Subsequent cooling below 660–600 °C (closure temperature of Pb diffusion in titanite) occurred between ca. 550 Ma and 540 Ma as indicated by dates obtained from smaller titanite

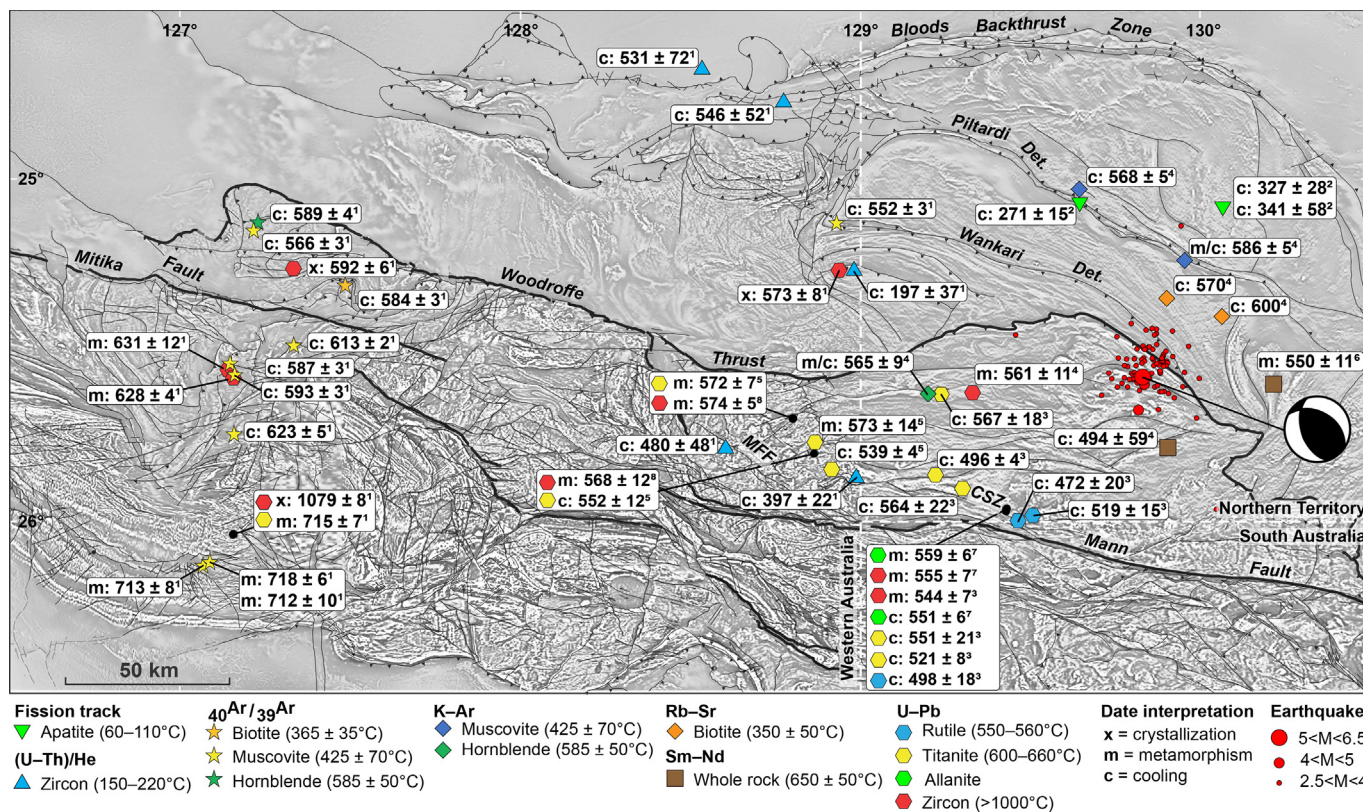


**Figure 7.** Thermochronology data for the western Musgrave Province (superscript numbers relate to references in Table 1), superimposed on a first vertical derivative total magnetic intensity (1VD-TMI) image. Also shown are interpreted structures, and the location of epicentres for the May 2016 earthquake. The preferred magnitude is  $M_w$  (P-wave magnitude) of 6.1 (Geoscience Australia; <http://www.ga.gov.au/earthquakes/getQuakeDetails.do?quakeId=3822278&orid=1316703&sta=WRKA>) and the resolved focal mechanism shown for the main shock is from data from GEOSCOPE, IGP website (<http://geoscope.ipgp.fr/index.php/en/catalog/earthquake-description?seis=us10005iyk>) using the SCARDEC method (Vallée et al., 2010; Vallée, 2013). MFF: Mount Fanny Fault; CSZ: Cockburn Shear Zone.

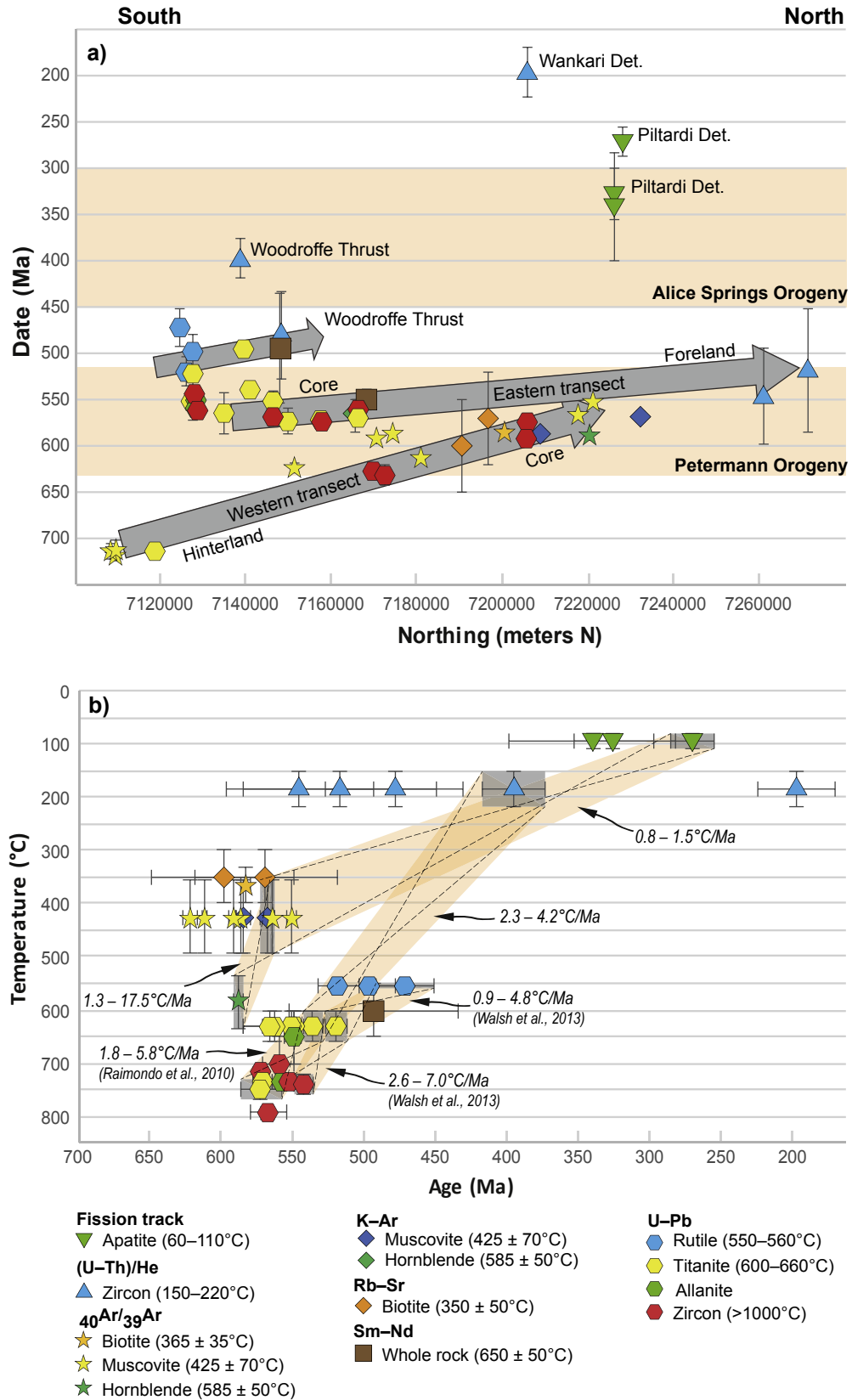


**Figure 8.** Summary plots of thermochronology data for the western Musgrave Province. (a) Thermochronology data plotted against UTM northing, the large arrows show the overall younging of ages towards the north, from the hinterland to the core for the western transect, and from the core to the foreland for the eastern transect. Shaded fields indicate the age ranges of the Alice Springs and Petermann Orogenies. (b) Estimated temperature vs. age showing average cooling rates from published data (superscript numbers relate to references of Table 1) as well as from new data. See text for full explanation.

grains (Raimondo et al., 2009). New  $^{40}\text{Ar}/^{39}\text{Ar}$  data from muscovite, from the Dog Leg Anticline, a regional scale fold affecting the Wankari/Piltardi Detachment in the foreland fold and thrust belt, indicate cooling below ca. 425 °C at  $552 \pm 3$  Ma (Figs. 2 and 7). This date is slightly younger than K–Ar dates of  $568 \pm 5$  Ma and  $586 \pm 5$  Ma for muscovite 70–100 km to the east (Scrimgeour et al., 1999), on the northern limb of the Dog Leg Anticline (Fig. 7). The Dog Leg Anticline is a late stage fold that affected the pre-existing Wankari/Piltardi Detachment system (Forman, 1966; Scrimgeour et al., 1999; Flöttmann et al., 2004). This indicates that the early stages of development of the thrust system of the Petermann Nappe Complex were followed by younger, out-of-sequence, internal deformation. Although the older dates may reflect exhumation related to development of the Wankari/Piltardi Detachment system, the younger date may reflect the time of cooling, either synchronous with or after formation of the Dog Leg Anticline. Alternatively, the ca. 552 Ma date could reflect a mixed age resulting from slow cooling or partial resetting.

Zircon (U–Th)/He thermochronology from the northern end of the Petermann Nappe Complex yielded cooling ages of ca. 545 Ma and ca. 520–530 Ma that broadly fall within the age of the Petermann Orogeny, although the large uncertainties on these dates do not allow for precise dating of movement within the thrust system (Figs. 7 and 8a). Zircon (U–Th)/He data from the core of the orogen, show that different areas cooled below 150–220 °C at ca. 480 Ma and ca. 400 Ma (Figs. 7 and 8a). Although the large uncertainty ( $\pm 48$  Ma) on the ca. 480 Ma date does not permit definitive discrimination from cooling related to the Petermann Orogeny, the smaller uncertainty on the younger date (i.e.  $397 \pm 22$  Ma) reflects an age that falls within the 450–295 Ma Alice Springs Orogeny. This implies that exhumation to shallow crustal levels largely postdated the Petermann Orogeny and may represent far field reactivation of the Woodroffe Thrust during the 450–295 Ma Alice Springs Orogeny (Fig. 8a). In the foreland fold and thrust belt, apatite fission track data from samples collected 70–120 km east of our study area, on the northern side of the Wankari/Piltardi Detachment, yielded dates of 341–271 Ma, interpreted as cooling ages (Tingate, 1990; Edgoose et al., 2004). This reflects exhumation of the Petermann Nappe Complex to shallow crustal levels during the latest stages of the Alice Springs Orogeny (Figs. 7 and 8a; Tingate, 1990; Edgoose et al., 2004). A single zircon (U–Th)/He date south of the Wankari Detachment implies that internal deformation of the fold and thrust belt occurred until ca. 200 Ma with substantial exhumation along the Wankari detachment (Figs. 7 and 8a).

#### 4.2. Active seismicity

On May 21, 2016 (Sydney date), a magnitude 6.1 earthquake in the Petermann Ranges produced a 20 km long surface rupture with ground displacement of up to 1 m (Fig. 7, Geoscience Australia website). This is the largest earthquake in Australia since 1997, and the largest ever recorded in the Musgrave Province. This earthquake was preceded by a magnitude 3.5 foreshock two days earlier and followed by 73 aftershocks ranging from magnitude 2.8 to 4.1 in the following six months (Fig. 7). Epicentres for the main earthquake, foreshock, and most aftershocks are located within 10 km southwest of the Woodroffe Thrust (Fig. 7). Depth estimates for the hypocentres are  $<1$  km, indicating that these earthquake events were most likely related to movement on the gently southwest-dipping Woodroffe Thrust (Fig. 7). The resolved focal mechanism for the main shock indicates compressive stress along northwest-striking structures (Fig. 7; SCARDEC data, Vallée et al., 2010; Vallée, 2013), demonstrating that thrusting and exhumation along the Woodroffe Thrust or associated splays is ongoing.

This recent seismic activity is not isolated. Prior to the 2016 event, five  $M > 5$  earthquakes occurred in the Musgrave Province between 1986 and 2016 with focal mechanisms indicative of thrusting and strike-slip faulting. All solutions indicate horizontal maximum stress and at least two major thrusting events are due to movement on the Woodroffe Thrust (Geoscience Australia website). More recently, on April 14, 2017 (Sydney date), the epicentre of a M4.3 earthquake was recorded just 10 km south of the M6.1 earthquake. This relatively abundant seismic activity on major structures of the Musgrave Province indicates transmission of tectonic stress from the northern Indo–Australia Plate boundary into the continent interior and localization of deformation along pre-existing structures, reinforcing the role of structural inheritance in strain localization.

#### 4.3. Cooling rate

Table 1 provides a compilation of new and previously published thermochronology data for the western Musgrave Province (Fig. 7). Fig. 8b shows estimated temperatures for each isotopic date, so that the slopes of dashed lines between two data points graphically represent cooling rates. The uncertainties associated with dates and temperatures are represented by the grey rectangles around symbols and the uncertainties in averaged cooling rates can be estimated by intersecting dashed lines, linking opposite corners of the rectangles (Fig. 8b).

Published cooling rates from the core of the Petermann Orogen (Bates region, Cockburn Shear Zone and Western Mann Region) range of 0.9–7.0 °C/Ma (Fig. 8b; Raimondo et al., 2010; Walsh et al., 2013). The pervasive mylonitic fabric of the orogenic core (the area around Mount Daisy Bates bounded by the Mann Fault and the Woodroffe Thrust) formed at subeclogite facies conditions (10–14 kbar; 700–800 °C) and peak metamorphic conditions were attained at ca. 570 Ma as indicated by SIMS (SHRIMP) zircon and titanite U–Pb dates (Table 1; Figs. 7 and 8b; Raimondo et al., 2009; Raimondo et al., 2010). Peak metamorphic conditions were followed by slow cooling to 600–660 °C at 540 Ma at  $\sim 1.8$ –5.8 °C/Ma (Fig. 8b) (Raimondo et al., 2010). U–Pb zircon data for samples collected in the core of the orogen, 40–60 km east of the Raimondo et al. (2010) study area suggest that peak metamorphic temperatures of 720–760 °C (Ti-in-zircon thermometry data) were attained at  $544 \pm 7$  Ma (Table 1; Figs. 7 and 8b; Walsh et al., 2013). U–Pb titanite data indicate that temperatures of 600–660 °C were attained at ca. 521 Ma, suggesting cooling of 2.6–7.0 °C/Ma (Fig. 8b; Walsh et al., 2013). U–Pb analyses of rutile indicate further cooling to 550–560 °C at 498–472 Ma at a rate of 0.9–4.8 °C/Ma (Fig. 8b; Walsh et al., 2013). These prolonged and relatively slow cooling rates, together with the existence of regional-scale, flat-lying mylonitic fabrics with opposing senses of shear, are consistent with exhumation of the core of the orogen in a crustal channel flow zone between the Woodroffe Thrust and the Mann Fault (Raimondo et al., 2009, 2010; Walsh et al., 2013).

A zircon (U–Th)/He date of ca. 400 Ma, obtained from the same structural block and near the Raimondo et al. (2010) cooling age of ca. 540 Ma (600–660 °C), shows that subsequent cooling to 150–220 °C occurred at an average cooling rate of 2.3–4.2 °C/Ma (Figs. 7 and 8b). This is within the range of published values of 0.9–7.0 °C/Ma obtained from the core of the orogen (Raimondo et al., 2010; Walsh et al., 2013). The zircon (U–Th)/He date of ca. 480 Ma obtained west of the Mount Fanny Fault falls broadly within the rutile U–Pb dates of 498–472 Ma obtained east of the Cockburn Shear Zone and agree with the fault-controlled differential cooling of the orogenic core along strike proposed by Walsh et al. (2013) (Fig. 7). The crustal channel flow model suggested for the exhumation of the core of the orogen explains the slow cooling rates

observed at higher temperatures from ca. 700–800 °C to 600–660 °C and to 550–560 °C between ca. 570 Ma and 470 Ma, respectively (Raimondo et al., 2009, 2010; Walsh et al., 2013). Further cooling to 150–220 °C occurred at a similar rate between ca. 480 Ma and 400 Ma.

From the western transect, the average cooling rate of the core of the orogen can be estimated using the time of cooling below 585 ± 50 °C ( $^{40}\text{Ar}/^{39}\text{Ar}$  hornblende) at 589 ± 4 Ma and cooling below 425 ± 70 °C ( $^{40}\text{Ar}/^{39}\text{Ar}$  muscovite) at 566 ± 3 Ma (Figs. 7 and 8b). This results in an average cooling rate of 1.3–17.5 °C/Ma, comparable values to those from the core of the orogen, ca. 150 km to the east.

Published data from the Piltardi Detachment indicate cooling below ca. 425 °C (K–Ar muscovite) at 568 ± 5 Ma (Scrimgeour et al., 1999), followed by subsequent cooling through the partial annealing zone of 60–120 °C of the apatite fission track method at 271 ± 15 Ma (Tingate, 1990). If the K–Ar date is correct, this implies a low average cooling rate of 0.8–1.5 °C/Ma (Fig. 8b); such a low rate could be interpreted as the result of erosional denudation. However, the zircon (U–Th)/He date of 197 ± 37 Ma is interpreted as the time of cooling through the He partial retention zone in zircon, and similar single dates from this sample at low and high effective uranium content (eU) values (Fig. 6), in addition to the apatite fission track date of ca. 271 Ma may suggest rapid cooling through the 220–60 °C temperature range, which may reflect tectonic exhumation. If correct, this implies that the average exhumation rate of 0.8–1.5 °C/Ma represents very slow tectonic exhumation within the Piltardi Detachment during reactivation of the foreland fold and thrust belt of the Petermann Orogen.

#### 4.4. On the duration of intraplate deformation, cratonization and plate tectonics

Structural and thermochronology data from the west Musgrave Province show interspersed compressional episodes between ca. 715 Ma and 200 Ma, indicating a timing of amagmatic intracontinental reactivation spanning approximately ca. 500 Million years. Focal mechanisms of recent earthquakes suggest that horizontal compression is ongoing, resulting in thrusting and strike-slip faulting in the Musgrave Province. Taken together, this shows that amagmatic reactivation of the Musgrave Province has been occurring over the past ca. 715 Ma.

Examples of intracontinental reactivation have been demonstrated in several Australian Precambrian and Phanerozoic orogens. The Capricorn Orogen and the Musgrave Province record a remarkably prolonged history of intracontinental reactivation. More than one billion years of intraplate crustal reworking has been identified in the Capricorn Orogen, including the 1820–1770 Ma Capricorn Orogeny, the 1680–1620 Ma Mangaroon Orogeny, the 1321–1171 Ma Mutherbukin Tectonic Event, the 1030–955 Ma Edmondian Orogeny, and the ca. 570 Ma Mulka Tectonic Event (Johnson et al., 2013, 2017; Korhonen and Johnson, 2015; Korhonen et al., 2017). The Musgrave Province evolved in an intraplate setting from the end of the 1310–1293 Ma Mount West Orogeny. It was then affected by the 1220–1150 Ma Musgrave Orogeny, which was closely followed by the 1085–1030 Ma Giles Event (Howard et al., 2015; Smithies et al., 2015b). Finally, the Musgrave Province was reactivated during the younger events described in this paper, including the 630–520 Ma Petermann Orogeny. Most of these examples were accompanied by voluminous magmatism, with the younger events being amagmatic. Other amagmatic intraplate compressional events in Australia include the ca. 550 Ma King Leopold Orogeny, marginal orogen of the Kimberley Basin and the 450–300 Ma Alice Springs Orogeny of the southern Arunta Province. It appears that the late stages of evolution of the Proterozoic–Phanerozoic orogens of Australia were largely

amagmatic tectonic events, possibly indicating an evolution towards cratonization. Commonly, these events last tens of millions of years and up to ca. 150 Ma. Comparatively, the ca. 715 Ma of amagmatic intracontinental reactivation of the Musgrave Province is extremely prolonged and challenges the concept of cratonization.

The cratonization of continental crust is the result of cumulative processes that ultimately lead to a thermally and mechanically stable crust (Rudnick and Fountain, 1995; Sandiford and McLaren, 2002; Johnson et al., 2017). Cratons are often referred to as the non-deformable portions of the continental lithosphere and this is commonly viewed as resulting from a lower crust depleted in heat producing elements (HPEs; Rudnick and Fountain, 1995). The depletion in HPEs is often attributed to chemical differentiation during partial melting and the migration of HPEs into the melt, leaving behind a granulite-facies residue depleted in HPEs (Sandiford and McLaren, 2002; Johnson et al., 2017). If no addition of juvenile material occurs, then successive magmatic events should theoretically lead to progressive cratonization (Johnson et al., 2017). However, Alessio et al. (2018) showed that HPE ratios remained constant during progressive metamorphism and partial melting, and that melt extraction does not reduce the concentration of HPEs in residual granulite-facies rocks of the lower crust. This suggests that chemical differentiation during partial melting is not the sole process responsible for cratonization, and that the decrease in crustal heat production rate with increasing depth in the crust simply reflects the relative lack of HPE-rich lithologies—i.e. the abundance of mafic rocks—in the deep crust (Alessio et al., 2018). This implies that addition of large amounts of mafic material into the crust reduces the overall heat production of the crust through time, and therefore, favours cratonization. The 1085–1030 Ma Giles Event is a world-class example of the addition of huge volumes of mafic material into the crust. The Musgrave Province, however, underwent some ca. 715 Ma of reactivation, with peak metamorphic conditions approaching eclogite facies at ca. 570 Ma during the Petermann Orogeny, approximately 460 Ma after the end of the Giles Event. This relative timing suggests that mafic melt addition into the crust alone is insufficient to cratonize the crust, or alternatively, that other factors can compete with the net reduction of HPEs and hinder cratonization.

Rather, the reactivation and non-cratonization of a continental interior appear to result from a combination of factors, including in-plane tectonic stress transmission from the plate boundaries, structural inheritance (i.e. mechanical weaknesses), radiogenic heating, fluid-rock interaction and thick sedimentary blanketing (Sandiford and Hand, 1998; Hand and Sandiford, 1999; Raimondo et al., 2014; Korhonen et al., 2017). These factors compete with progressive cooling and cratonization of the crust, and are evidently efficient enough to produce intracontinental compressional orogens comparable in size to their plate margins counterparts. A combined thermo-mechanical numerical modelling approach would be a useful test of the minimum threshold values required for the initiation and sustainability of intracontinental orogeny. These experimental results could then be compared to the values for the key parameters identified in natural examples. Such an approach may aid elucidate the processes of far-field, in-plane horizontal stress transmission and strain localization resulting in a prolonged duration of intracontinental compressional orogeny which attains subeclogite facies peak metamorphic conditions.

Soon after the theory of Plate Tectonics was proposed, geologists working in continental settings rapidly expressed the need to define Continental Tectonics as a counterpart to the rigid plate paradigm of Plate Tectonics. Indeed the broad deformation zones of continental orogens contrast with the narrow plate boundaries implied by the rigid-plate paradigm. One approach was to consider the continental lithosphere as a series of rigid microplates moving

relative to one another along lithospheric faults acting like mini plate boundaries, as implied by the lateral extrusion model for Southeast Asia of [Tapponnier et al. \(1982\)](#). [Molnar \(1988\)](#) in his contribution: “*Continental tectonics in the aftermath of Plate Tectonics*” addressed the fact that buoyant continental crustal blocks can be detached from the mantle to form broad zones of diffuse deformation. Taken to the extreme, zones of diffuse deformation can be described by continuum dynamics that consider the crust to behave like a high viscosity fluid over long periods of time ([England and McKenzie, 1982](#)). Continuum dynamics explains the deformation continuum observed from a plate margin, progressively dissipating into the continental crust over large distances. However, in the case of intracontinental compressional orogeny, where no deformation continuum from the plate boundary to the intracontinental orogenic zone is observed, suggests that some parts of the continental lithosphere act as rigid blocks where in-plane horizontal stress is transmitted from the plate margin into a weakened intracontinental zone that can accommodate strain.

In past decades, the scientific community considered that Plate Tectonics was only fully valid in the oceanic setting where plate boundaries are narrow. Recently, [Crameri et al. \(2018\)](#) wrote “We find that the full range of dynamic behaviour of the oceanic plate, including its forcing and overall framework within Earth’s connecting system, is not fully captured by the existing concept of Plate Tectonics, which describes solely the horizontal surface kinematics of all plates. Therefore, we introduce a more specific and at the same time more integral concept named “Ocean-Plate Tectonics” that more specifically describes the dynamic life of the oceanic plate”. In the light of new data, the undisputable advances made using the rigid-plate paradigm of Plate Tectonics are viewed now as an oversimplification in both the continental and oceanic settings. This is largely expressed by the broad zones of deformation in continental settings but more spectacularly, the case of intracontinental compressional orogens, lacking a deformation continuum from the plate boundary into the continental interior, are a strong expression of the complexity of Continental Tectonics.

## 5. Conclusion

This study shows evidence for prolonged amagmatic intracontinental compression in central Australia, following a prolonged history of Mesoproterozoic tectonomagmatic events. Amagmatic intracontinental compression started as early as ca. 715 Ma and continued to the present day. Two previously unrecognised metamorphic events were identified from the western end of the Musgrave Province and dated at ca. 715 Ma (U–Pb titanite and  $^{40}\text{Ar}/^{39}\text{Ar}$  muscovite ages) and ca. 630 Ma (U–Pb zircon ages). These events are significantly older than the commonly accepted age range of 580–520 Ma for the Petermann Orogeny. Continuous tectonic exhumation from ca. 623 Ma to 565 Ma ( $^{40}\text{Ar}/^{39}\text{Ar}$  muscovite, biotite and hornblende ages) along structures including the Woodroffe Thrust and the Mitika Fault suggests continuous tectonism, forming the rationale for redefinition of the age range for the Petermann Orogeny to 630–520 Ma. Previously published U–Pb zircon and titanite data from the core of the orogen suggest that peak metamorphic conditions (10–14 kbars; 700–800 °C) were attained at ca. 570 Ma ([Gregory et al., 2009](#); [Raimondo et al., 2009, 2010](#); [Walsh et al., 2013](#)).  $^{40}\text{Ar}/^{39}\text{Ar}$  muscovite and (U–Th)/He zircon data show minimum ages for the development and internal deformation of the foreland fold and thrust belt (the Petermann Nappe Complex) of ca. 552 Ma to 520 Ma. Exhumation of the core of the Petermann Orogen to shallow crustal levels during reactivation of the Woodroffe Thrust occurred between ca. 480 Ma and 400 Ma, possibly as a response to shortening during the 450–300 Ma Alice Springs Orogeny. Slow averaged exhumation rates of 0.9–7 °C/Ma

appear to have prevailed from ca. 570 Ma to 400 Ma in the core of the orogen. Reactivation and exhumation of the hanging wall of the Wankari Detachment to shallow crustal levels is dated at ca. 200 Ma by (U–Th)/He zircon. The Musgrave Province is seismically active with five  $M > 5$  earthquakes along the Woodroffe Thrust and associated structures between 1986 and 2016. All indicate horizontal maximum stress, the most prominent of which occurred in May 2016 with a P-wave magnitude of 6.1 creating a surface rupture of 20 km with vertical ground displacement up to one meter and a resolved focal mechanism indicating thrusting demonstrating that deformation of the Australian continent interior is continuing to this day. Nowadays, the convergent plate margin is about 2000–2500 km north of the Musgrave Province, where the Indo-Australian plate subducts under the Banda Arc and collides with northern Papua New Guinea and the Ontong–Java Plateau. Intracontinental compression resulting from far-field stress at this convergent boundary gives insights into processes of in-plane stress transmission through the continental lithosphere that can serve as analogue for past intracontinental orogens.

The long-lived, amagmatic, intracontinental reactivation of central Australia is a remarkable example of stress transmission, strain localization and cratonization-hindering processes that highlights the complexity of Continental Tectonics with regards to the rigid-plate paradigm of Plate Tectonics. In the case of intracontinental compressional orogens, stress is transmitted through the continental lithosphere and strain is localised in the continental interior. No deformation continuum from the plate margin to the continental interior is observed, implying that some parts of the continental lithosphere act as rigid blocks where in-plane horizontal stress is transmitted with minimal loss. Strain localization occurs where it can be accommodated in a region of weakened continental lithosphere. This suggests that there are factors capable of hindering cratonization, such as structural inheritance, radiogenic heating, fluid-rock interaction and thick sedimentary blanketing as discussed by [Raimondo et al. \(2014\)](#). These mechanisms of stress transmission and strain localization still need to be tested by thermomechanical modelling using the range of values for the key parameters that have been observed in natural examples.

## Acknowledgements

The Ngaanyatjarra people are thanked for allowing us access to the land. Adam Symonds is thanked for helping with the drafting of figures. The thermochronology reported in this paper was conducted within the John de Laeter Centre at Curtin University, which is supported by the AuScope Earth Composition and Evolution program. RQdG, HMH, RHS, MTDW publish with the permission of the Executive Director of the Geological Survey of Western Australia. M.D. was supported by the AuScope NCRIS2 program, Australian Scientific Instruments Pty Ltd., Australian Research Council (ARC) Discovery funding scheme (DP160102427) and Curtin Research Fellowship. Stijn Glorie and an anonymous reviewer are thanked for providing reviews of the paper.

## Appendix A. Supplementary data

Supplementary data to this article can be found online at <https://doi.org/10.1016/j.gsf.2018.09.003>.

## References

- Aitken, A.R.A., Betts, P.G., Ailleres, L., 2009a. The architecture, kinematics, and lithospheric processes of a compressional intraplate orogen occurring under Gondwana assembly: the Petermann Orogeny, central Australia. *Lithosphere* 1 (6), 343–357.

- Aitken, A.R.A., Betts, P.G., Weinberg, R.F., Gray, D.J., 2009b. Constrained potential field modeling of the crustal architecture of the Musgrave Province in central Australia: evidence for lithospheric strengthening due to crust–mantle boundary uplift. *Journal of Geophysical Research* 114 (B12). <https://doi.org/10.1029/2008JB006194>.
- Alessio, K.L., Hand, M., Kelsey, D.E., Williams, M.A., Morrissey, L.J., Barovich, K., 2018. Conservation of deep crustal heat production. *Geology* 46 (4), 335–338. <https://doi.org/10.1130/G39970.1>.
- Bell, T.H., 1978. Progressive deformation and reorientation of fold axes in a ductile mylonite zone: the woodroffe thrust. *Tectonophysics* 44 (1–4), 285–320.
- Camacho, A., 1997. An isotopic study of deep-crustal orogenic processes, Musgrave Block, Central Australia. Australian National University, Canberra, Australian Capital Territory [PhD thesis] (unpublished).
- Camacho, A., Fanning, C.M., 1995. Some isotopic constraints on the evolution of the granulite and upper amphibolite facies terranes in the eastern Musgrave block, central Australia. *Precambrian Research* 71, 155–172.
- Camacho, A., McDougall, I., 2000. Intracratonic, strike-slip partitioned transpression and the formation of eclogite facies rocks: an example from the Musgrave Block, central Australia. *Tectonics* 19, 978–996.
- Close, D.F., Scrimgeour, I.R., Edgoose, C.J., 2003. Compilation of Geochronological Data from the Northwestern Musgrave Block, Northern Territory: Northern Territory Geological Survey, Technical Report 2003-006, 39p.
- Cramer, F., Conrad, C.P., Montési, L., Lithgow-Bertelloni, C.R., 2018. The dynamic life of an oceanic plate. *Tectonophysics*. <https://doi.org/10.1016/j.tecto.2018.03.016> (in press).
- Danišik, M., Fodor, L., Dunkl, I., Gerdes, A., Csizmeg, J., Hámor-Vidó, M., Evans, N.J., 2015. A multi-system geochronology in the Ad-3 borehole, Pannonian Basin (Hungary) with implications for dating volcanic rocks by low-temperature thermochronology and for interpretation of (U–Th)/He data. *Terra Nova* 27 (4), 258–269.
- De Grave, J., Buslov, M.M., Van den haute, P., 2007. Distant effects of India–Eurasia convergence and Mesozoic intracontinental deformation in Central Asia: constraints from apatite fission-track thermochronology. *Journal of Asian Earth Sciences* 29 (2–3), 188–204.
- Dewey, J.F., Bird, J.M., 1970. Mountain belts and the new global tectonics. *Journal of Geophysical Research* 75 (14), 2625–2647.
- Edgoose, C.J., Scrimgeour, I.R., Close, D.F., 2004. Geology of the Musgrave Block, Northern Territory. Northern Territory Geological Survey, Report 15, 46p.
- England, P., McKenzie, D., 1982. A thin viscous sheet model for continental deformation. *Geophysical Journal of the Royal Astronomical Society* 70 (2), 295–321.
- Evins, P.M., Kirkland, C.L., Wingate, M.T.D., Smithies, R.H., Howard, H.M., Bodorkos, S., 2012. Provenance of the 1340–1270 Ma Ramarama Basin in the West Musgrave Province. Geological Survey of Western Australia, Central Australia. Report 116, 39p.
- Evins, P.M., Smithies, R.H., Howard, H.M., Kirkland, C.L., Wingate, M.T.D., Bodorkos, S., 2010. Devil in the detail; the 1150–1000 Ma magmatic and structural evolution of the Ngaanyatjarra Rift, west Musgrave province, central Australia. *Precambrian Research* 183, 572–588.
- Flöttmann, T., Hand, M., Close, D.F., Edgoose, C., Scrimgeour, I.R., 2004. Thrust tectonic styles of the intracratonic Alice Springs and Petermann orogens, central Australia. In: McClay, K.R. (Ed.), *Thrust Tectonics and Hydrocarbon Systems*. American Association of Petroleum Geologists, pp. 538–557. Memoir 82.
- Forman, D.J., 1966. The Geology of the South-western Margin of the Amadeus Basin. Bureau of Mineral Resources, Central Australia. Report 87, 54p.
- Frost, B.R., Chamberlain, K.R., Schumacher, J.C., 2001. Sphene (titanite): phase relations and role as a geochronometer. *Chemical Geology* 172 (1), 131–148.
- Glikson, A.Y., Stewart, A.J., Ballhaus, C.G., Clarke, G.L., Feeken, E.H.T., Leven, J.H., Sheraton, J.W., Sun, S.S., 1996. Geology of the Western Musgrave Block, Central Australia, With Particular Reference to the Mafic–Ultramafic Giles Complex. Australian Geological Survey Organisation. Bulletin 239, 206p.
- Glorie, S., Agostino, K., Dutch, R., Pawley, M., Hall, J., Danišik, M., Evans, N.J., Collins, A.S., 2017. Thermal history and differential exhumation across the eastern Musgrave province, south Australia: insights from low-temperature thermochronology. *Tectonophysics* 703–704, 23–41.
- Gorczyk, W., Hobbs, B., Gessner, K., Gerya, T., 2013. Intracratonic geodynamics. *Gondwana Research* 24 (3–4), 838–848.
- Gorczyk, W., Smithies, H., Korhonen, F., Howard, H., Quentin de Gromard, R., 2015. Ultra-hot Mesoproterozoic evolution of intracontinental central Australia. *Geoscience Frontiers* 6 (1), 23–37.
- Gray, C.M., 1978. Geochronology of granulite-facies gneisses in the western Musgrave block, central Australia. *Journal of the Geological Society of Australia* 25, 403–414.
- Gregory, C.J., Buick, I.S., Hermann, J., Rubatto, D., 2009. Mineral-scale trace element and U–Th–Pb age constraints on metamorphism and melting during the Petermann Orogeny (Central Australia). *Journal of Petrology* 50 (2), 251–287. <https://doi.org/10.1093/petrology/egn077>.
- Hand, M., Sandiford, M., 1999. Intraplate deformation in central Australia, the link between subsidence and fault reactivation. *Tectonophysics* 305 (1–3), 121–140.
- Howard, H.M., Quentin de Gromard, R., Smithies, R.H., 2014. Warburton Range, WA Sheet 4245. Geological Survey of Western Australia, 1:100 000 Geological Series.
- Howard, H.M., Quentin de Gromard, R., Smithies, R.H., Werner, M., 2013. Bentley, WA Sheet 4346. Geological Survey of Western Australia, 1:100 000 Geological Series.
- Howard, H.M., Smithies, R.H., Kirkland, C.L., Evins, P.M., Wingate, M.T.D., 2009. Age and Geochemistry of the Alcurra Suite in the Western Musgrave Province and Implications for Orthomagmatic Ni–Cu–PGE Mineralization during the Giles Event. Geological Survey of Western Australia. Record 2009/16, 16p.
- Howard, H.M., Smithies, R.H., Kirkland, C.L., Kelsey, D.E., Aitken, A., Wingate, M.T.D., Quentin de Gromard, R., Spaggiari, C.V., Maier, W.D., 2015. The burning heart — the Proterozoic geology and geological evolution of the west Musgrave Region, central Australia. *Gondwana Research* 27 (1), 64–94.
- Howard, H.M., Smithies, R.H., Pirajno, F., 2007. Geochemical and Nd isotopic signatures of mafic dykes in the western Musgrave Complex. In: Geological Survey of Western Australia Annual Review 2005–06. Geological Survey of Western Australia, Perth, Western Australia, pp. 64–71.
- Jessell, M.W., 1987. Grain-boundary migration microstructures in a naturally deformed quartzite. *Journal of Structural Geology* 9 (8), 1007–1014.
- Johnson, S.P., Korhonen, F.J., Kirkland, C.L., Cliff, J.B., Belousova, E.A., Sheppard, S., 2017. An isotopic perspective on growth and differentiation of Proterozoic orogenic crust: from subduction magmatism to cratonization. *Lithos* 268–271, 76–86.
- Johnson, S.P., Thorne, A.M., Tyler, I.M., Korsch, R.J., Kennett, B.L.N., Cutten, H.N., Goodwin, J., Blay, O.A., Blewett, R.S., Joly, A., Dentith, M.C., Aitken, A.R.A., Holzschuh, J., Salmon, M., Reading, A., Heinson, G., Boren, G., Ross, J., Costelloe, R.D., Fomin, T., 2013. Crustal architecture of the capricorn orogen, western Australia and associated metallogeny. *Australian Journal of Earth Sciences* 60 (6–7), 681–705. <https://doi.org/10.1080/08120099.2013.826735>.
- Kirkland, C.L., Smithies, R.H., Spaggiari, C.V., 2015. Foreign contemporaries — unravelling disparate isotopic signatures from Mesoproterozoic Central and Western Australia. *Precambrian Research* 265, 218–231.
- Kirkland, C.L., Smithies, R.H., Spaggiari, C.V., Wingate, M.T.D., Quentin de Gromard, R., Clark, C., Gardiner, N.J., Belousova, E.A., 2017. Proterozoic crustal evolution of the Eucla basement, Australia: implications for destruction of oceanic crust during emergence of Nuna. *Lithos* 278, 427–444.
- Kirkland, C.L., Smithies, R.H., Woodhouse, A.J., Howard, H.M., Wingate, M.T.D., Belousova, E.A., Cliff, J.B., Murphy, R.C., Spaggiari, C.V., 2013. Constraints and deception in the isotopic record; the crustal evolution of the west Musgrave Province, central Australia. *Gondwana Research* 23 (2), 759–781.
- Korhonen, F.J., Johnson, S.P., 2015. The role of radiogenic heat in prolonged intraplate reworking: the capricorn orogen explained? *Earth and Planetary Science Letters* 428, 22–32.
- Korhonen, F.J., Johnson, S.P., Wingate, M.T.D., Kirkland, C.L., Fletcher, I.R., Dunkley, D.J., Roberts, M.P., Sheppard, S., Muhling, J.R., Rasmussen, B., 2017. Radiogenic heating and craton–margin plate stresses as drivers for intraplate orogeny. *Journal of Metamorphic Geology* 35 (6), 631–661. <https://doi.org/10.1111/jmg.12249>.
- Kruhl, J.H., 1996. Prism- and basal-plane parallel subgrain boundaries in quartz: a microstructural geothermobarometer. *Journal of Metamorphic Geology* 14 (5), 581–589.
- Lambeck, K., Burgess, G., 1992. Deep crustal structure of the Musgrave Block, central Australia: results from teleseismic travel-time anomalies. *Australian Journal of Earth Sciences* 39, 1–20.
- Major, R.B., Connor, C.H.H., 1993. Musgrave block. In: Drexel, J.F., Preiss, W.V., Parker, A.J. (Eds.), *The Geology of South Australia*. Geological Survey of South Australia, pp. 156–167. Bulletin 54.
- Mansurov, A.N., 2017. A continuum model of present-day crustal deformation in the Pamir-Tien Shan region constrained by GPS data. *Russian Geology and Geophysics* 58 (7), 787–802.
- Marshall, S., Karlstrom, K.E., Timmons, J.M., 2000. Inversion of Proterozoic extensional faults: an explanation for the pattern of Laramide and Ancestral Rockies intracratonic deformation, United States. *Geology* 28 (8), 735–738.
- McKenzie, D., Parker, R., 1967. The North Pacific: an example of tectonics on a sphere. *Nature* 216, 1276.
- Molnar, P., Tapponnier, P., 1975. Cenozoic tectonics of Asia: effects of a continental collision. *Science* 189 (4201), 419.
- Molnar, P., 1988. Continental tectonics in the aftermath of plate tectonics. *Nature* 335, 131.
- Nicolas, M., Sautoire, J.P., Delpech, P.Y., 1990. Intraplate seismicity: new seismotectonic data in Western Europe. *Tectonophysics* 179 (1), 27–53.
- Passchier, C.W., Trouw, R.A.J., 1996. *Microtectonics*. Springer-Verlag, Berlin, 289p.
- Pfiffner, O.A., 2009. Evolution of the north alpine foreland basin in the central Alps. In: Allen, P.A., Homewood, P. (Eds.), *Foreland Basins*, pp. 219–228.
- Quentin de Gromard, R., Howard, H.M., Kirkland, C.L., Smithies, R.H., Wingate, M.T.D., Jourdan, F., 2017a. Post-Giles Event evolution of the Musgrave province constrained by (multi-method) thermochronology. In: GSWA 2017 Extended Abstracts: Promoting the Prospectivity of Western Australia: Geological Survey of Western Australia, Record 2017/2, pp. 42–47.
- Quentin de Gromard, R., Howard, H.M., Smithies, R.H., 2015. Golden Point, WA Sheet 4246. Geological Survey of Western Australia, 1:100 000 Geological Series.
- Quentin de Gromard, R., Howard, H.M., Smithies, R.H., 2016a. Diorite, WA Sheet 4347. Geological Survey of Western Australia, 1:100 000 Geological Series.
- Quentin de Gromard, R., Howard, H.M., Smithies, R.H., Wingate, M.T.D., Lu, Y., 2017b. The Deep Seismic Reflection Profile 11GA-YO1 in the West Musgrave Province: an Updated View. Geological Survey of Western Australia. Record 2017/8, 20p.
- Quentin de Gromard, R., Wingate, M.T.D., Kirkland, C.L., Howard, H.M., Smithies, R.H., 2016b. Geology and U–Pb Geochronology of the Warlawurru Supersuite and MacDougall Formation in the Mitika and Wanarn Areas, West Musgrave Province. Geological Survey of Western Australia. Record 2016/4, 29p.
- Raimondo, T., Collins, A.S., Hand, M., Walker-Hallam, A., Smithies, R.H., Evins, P.M., Howard, H.M., 2009. Ediacaran intracontinental channel flow. *Geology* 37 (4), 291–294.

- Raimondo, T., Collins, A.S., Hand, M., Walker-Hallam, A., Smithies, R.H., Evins, P.M., Howard, H.M., 2010. The anatomy of a deep intracontinental orogen. *Tectonics* 29 (TC4024). <https://doi.org/10.1029/2009TC002504>.
- Raimondo, T., Hand, M., Collins, W.J., 2014. Compression intracontinental orogens: ancient and modern perspectives. *Earth-science Reviews* 130, 128–153.
- Reiners, P.W., Farley, K.A., Hickes, H.J., 2002. He diffusion and (U–Th)/He thermochronometry of zircon: initial results from Fish Canyon Tuff and Gold Butte. *Tectonophysics* 349 (1), 297–308.
- Reiners, P.W., Spell, T.L., Nicolescu, S., Zanetti, K.A., 2004. Zircon (U–Th)/He thermochronometry: He diffusion and comparisons with  $^{40}\text{Ar}/^{39}\text{Ar}$  dating. *Geochimica et Cosmochimica Acta* 68 (8), 1857–1887.
- Rudnick, R.L., Fountain, D.M., 1995. Nature and composition of the continental crust: a lower crustal perspective. *Review of Geophysics* 33, 267–309.
- Sandiford, M., Hand, M., 1998. Controls on the locus of intraplate deformation in Central Australia. *Earth and Planetary Science Letters* 162, 97–110.
- Sandiford, M., McLaren, S., 2002. Tectonic feedback and the ordering of heat producing elements within the continental lithosphere. *Earth and Planetary Science Letters* 204 (1–2), 133–150.
- Scibiorski, E., Tohver, E., Jourdan, F., 2015. Rapid cooling and exhumation in the western part of the mesoproterozoic Albany–fraser orogen, western Australia. *Precambrian Research* 265, 232–248.
- Scrimgeour, I.R., Close, D.F., 1999. Regional high pressure metamorphism during intracratonic deformation: the Petermann Orogeny, central Australia. *Journal of Metamorphic Geology* 17, 557–572.
- Scrimgeour, I.R., Close, D.F., Edgoose, C.J., 1999. Petermann Ranges, Northern Territory (2nd Edition). Northern Territory Geological Survey, 1:250 000 geological map series explanatory notes SC52-07, 59p.
- Searle, M.P., Elliott, J.R., Phillips, R.J., Chung, S.L., 2011. Crustal–lithospheric structure and continental extrusion of Tibet. *Journal of the Geological Society* 168 (3), 633–672. <https://doi.org/10.1144/0016-76492010-139>.
- Smithies, R.H., Howard, H.M., Evins, P.M., Kirkland, C.L., Bodorkos, S., Wingate, M.T.D., 2009. West Musgrave Complex — New Geological Insights from Recent Mapping, Geochronology, and Geochemical Studies. Geological Survey of Western Australia. Record 2008/19, 20p.
- Smithies, R.H., Howard, H.M., Evins, P.M., Kirkland, C.L., Kelsey, D.E., Hand, M., Wingate, M.T.D., Collins, A.S., Belousova, E., 2011. High-temperature granite magmatism, crust–mantle interaction and the Mesoproterozoic intracontinental evolution of the Musgrave province, Central Australia. *Journal of Petrology* 52 (5), 931–958.
- Smithies, R.H., Howard, H.M., Evins, P.M., Kirkland, C.L., Kelsey, D.E., Hand, M., Wingate, M.T.D., Collins, A.S., Belousova, E., Allchurch, S., 2010. Geochemistry, Geochronology, and Petrogenesis of Mesoproterozoic Felsic Rocks in the West Musgrave Province, Central Australia, and Implications for the Mesoproterozoic Tectonic Evolution of the Region. Geological Survey of Western Australia. Report 106, 73p.
- Smithies, R.H., Howard, H.M., Kirkland, C.L., Korhonen, F.J., Medlin, C.C., Maier, W.D., Quentin de Gromard, R., Wingate, M.T.D., 2015a. Piggy-back supervolcanoes — long-lived, voluminous, juvenile rhyolite volcanism in Mesoproterozoic central Australia. *Journal of Petrology* 56 (4), 735–763. <https://doi.org/10.1093/petrology/egv015>.
- Smithies, R.H., Kirkland, C.L., Korhonen, F.J., Aitken, A.R.A., Howard, H.M., Maier, W.D., Wingate, M.T.D., Quentin de Gromard, R., Gessner, K., 2015b. The Mesoproterozoic thermal evolution of the Musgrave province in central Australia — plume vs. the geological record. *Gondwana Research* 27 (4), 1419–1429. <https://doi.org/10.1016/j.gr.2013.12.014>.
- Stipp, M., Stünitz, H., Heilbronner, R., Schmid, S.M., 2002. The eastern Tonale fault zone: a 'natural laboratory' for crystal plastic deformation of quartz over a temperature range from 250 to 700°C. *Journal of Structural Geology* 24, 1861–1884.
- Tapponnier, P., Molnar, P., 1979. Active faulting and cenozoic tectonics of the tien Shan, Mongolia, and Baykal regions. *Journal of Geophysical Research: Solid Earth* 84 (B7), 3425–3459.
- Tapponnier, P., Peltzer, G., Le Dain, A.Y., Armijo, R., Cobbold, P., 1982. Propagating extrusion tectonics in Asia: new insights from simple experiments with plasticine. *Geology* 10 (12), 611–616. [https://doi.org/10.1130/0091-7613\(1982\)10<611:PETIAN>2.0.CO;2](https://doi.org/10.1130/0091-7613(1982)10<611:PETIAN>2.0.CO;2).
- Tingate, P., 1990. Apatite Fission Track Studies from the Amadeus Basin, Central Australia. Department of Geology, University of Melbourne, Melbourne [PhD thesis] (unpublished).
- Vallée, M., 2013. Source time function properties indicate a strain drop independent of earthquake depth and magnitude. *Nature Communications* 4, 2606.
- Vallée, M., Charléty, J., Ferreira, A.M.G., Delouis, B., Vergoz, J., 2010. SCARDEC: a new technique for the rapid determination of seismic moment magnitude, focal mechanism and source time functions for large earthquakes using body–wave deconvolution. *Geophysical Journal International* 184 (1), 338–358. <https://doi.org/10.1111/j.1365-246X.2010.04836.x>.
- van der Pluijm, B.A., Craddock, J.P., Graham, B.R., Harris, J.H., 1997. Paleostress in cratonic north America: implications for deformation of continental interiors. *Science* 277 (5327), 794.
- Walsh, A.K., Raimondo, T., Kelsey, D.E., Hand, M., Pfitzner, H.L., Clark, C., 2013. Duration of high-pressure metamorphism and cooling during the intraplate Petermann Orogeny. *Gondwana Research* 24 (3–4), 969–983. <https://doi.org/10.1016/j.gr.2012.09.006>.
- Wex, S., Mancktelow, N.S., Hawemann, F., Camacho, A., Pennacchioni, G., 2017. Geometry of a large–scale, low–angle, midcrustal thrust (Woodroffe Thrust, central Australia). *Tectonics* 36 (11), 2447–2476. <https://doi.org/10.1002/2017TC004681>.
- Wingate, M.T.D., Campbell, I.H., Compston, W., Gibson, G.M., 1998. Ion microprobe U–Pb ages for Neoproterozoic basaltic magmatism in south-central Australia and implications for the breakup of Rodinia. *Precambrian Research* 87 (3–4), 135–159. [https://doi.org/10.1016/S0301-9268\(97\)00072-7](https://doi.org/10.1016/S0301-9268(97)00072-7).
- Wingate, M.T.D., Pirajno, F., Morris, P.A., 2004. Warakurna large igneous province: a new Mesoproterozoic large igneous province in west-central Australia. *Geology* 32 (2), 105–108.
- Zoback, M.L., 1992. Stress field constraints on intraplate seismicity in eastern North America. *Journal of Geophysical Research: Solid Earth* 97 (B8), 11761–11782.
- Zoback, M.L., Zoback, M.D., Adams, J., Assumpcao, M., Bell, S., Bergman, E.A., Blumling, P., Brereton, N.R., Denham, D., Ding, J., Fuchs, K., Gay, N., Gregersen, S., Gupta, H.K., Gvishiani, A., Jacob, K., Klein, R., Knoll, P., Magee, M., Mercier, J.L., Muller, B.C., Paquin, C., Rajendran, K., Stephansson, O., Suarez, G., Suter, M., Udias, A., Xu, Z.H., Zhizhin, M., 1989. Global patterns of tectonic stress. *Nature* 341, 291.